

DESTRUCTION OF THE GALACTIC GLOBULAR CLUSTER SYSTEM

Oleg Y. Gnedin

and

Jeremiah P. Ostriker

Princeton University Observatory, Peyton Hall, Princeton, NJ 08544;
ognedin@astro.princeton.edu, jpo@astro.princeton.edu

ABSTRACT

We investigate the dynamical evolution of the Galactic Globular Cluster System in considerably greater detail than has been done hitherto, finding that destruction rates are significantly larger than given by previous estimates. The general scheme (but not the detailed implementation) follows Aguilar, Hut, & Ostriker (1988; AHO).

For the evolution of individual clusters we use a Fokker-Planck code including the most important physical processes governing the evolution: two-body relaxation, tidal truncation of clusters, compressive gravitational shocks while clusters pass through the Galactic disk, and tidal shocks due to passage close to the bulge. Gravitational shocks are treated comprehensively, using a recent result by Kundić & Ostriker (1995) that the $\langle \Delta E^2 \rangle$ shock-induced relaxation term, driving an additional dispersion of energies, is generally more important than the usual energy shift term $\langle \Delta E \rangle$. Various functional forms of the correction factor are adopted to allow for the adiabatic conservation of stellar actions in a presence of transient gravitational perturbation.

We use a recent compilation of the globular cluster positional and structural parameters, and a collection of radial velocity measurements. Two transverse to the line-of-sight velocity components were assigned randomly according to the two kinematic models for the cluster system (following the method of AHO): one with an isotropic peculiar velocity distribution, corresponding to the present day cluster population, and the other with the radially-preferred peculiar velocities, similar to those of the stellar halo. We use the Ostriker & Caldwell (1983) and the Bahcall, Schmidt, & Soneira (1983) models for our Galaxy.

For each cluster in our sample we calculated its orbits over a Hubble time, starting from the *present* observed positions and assumed velocities. Medians of the resulting set of peri- and apogalactic distances and velocities are used then

as an input for the Fokker-Planck code. Evolution of the cluster is followed up to its total dissolution due to a coherent action of all of the destruction mechanisms. The rate of destruction is then obtained as a median over all the cluster sample, in accord with AHO.

We find that the total destruction rate is much larger than that given by AHO with more than half of the present clusters (52% – 58% for the OC model, and 75% – 86% for the BSS model) destroyed in the next Hubble time. Alternatively put, the typical time to destruction is comparable to the typical age, a results that would follow from (but is not required by) an initially power law distribution of destruction times. We discuss some implications for a past history of the Globular Cluster System, and the initial distribution of the destruction times raising the possibility that the current population is but a very small fraction of the initial population with the remnants of the destroyed clusters constituting presently a large fraction of the spheroid (bulge+halo) stellar population.

Subject headings: celestial mechanics, stellar dynamics – globular clusters: general – Galaxy: kinematics and dynamics

1. Introduction

Globular clusters are thought to be the oldest stellar systems in our Galaxy, and a history of attempts by theoreticians and observers to understand the keys of their evolution is as old as the discipline of stellar dynamics, with a comprehensive review provided by Spitzer (1987). Yet, these relatively simple stellar systems are not understood well enough to predict their future with desirable accuracy, in part due to lack of accurate observational values for the current dynamical state and in part due to a residual uncertainty concerning the complete catalog of relevant physical processes operating on these systems. More than that, we have almost no clues about their past, and in particular, whether what we see now is representative of the *initial* Globular Cluster System, or just a small leftover after a great destruction battle that occurred earlier in the history of the Galaxy. In this paper we consider the evolution of the globular clusters and their ultimate disappearance, and propose a simple model for their initial distribution.

Pre- and post-core collapse evolution of an isolated cluster is relatively well understood (Spitzer 1987; Goodman 1993). Significant progress in understanding of the evolution was achieved using Monte Carlo and Fokker-Planck calculations. But the galactic environment

makes the clusters subject to external perturbations – tidal truncation and the gravitational shocks due to passages close to the bulge and through the disk. The shock processes, although known to be important, have never been carefully included in the evolution of the system. We investigate the Fokker-Planck models including the shocks elsewhere (Gnedin, Lee, & Ostriker 1996; hereafter GLO) and show that the dispersion of energy of the stars, induced by the shocks (Kundić & Ostriker 1995; hereafter KO), is generally even more important for the evolution than the first-order energy shift. Another very important aspect of modelling globular clusters is the initial mass spectrum. Multi-mass clusters undergo core collapse much faster than in the single-mass case, and their destruction is much more efficient (see Lee & Goodman 1995, and the references in GLO). We restrict ourselves however to the single mass models in order to maintain clear physical understanding; but due to omission of this aspect of the problem, our results provide a lower bound to the rate of destruction of the globular clusters.

As long as we have (at least, approximate) understanding of the evolution of a single cluster we can turn to the study of the system of globular cluster in our Galaxy, and in external galaxies. Chernoff, Kochanek, & Shapiro (1986) used a semi-analytical Monte-Carlo technique to estimate the importance of the different mechanisms acting upon the cluster. They considered two-body relaxation, tidal stripping of stars, and the first order tidal shocking effect - due to the crossing disk and interactions with giant molecular clouds (GMC). For each of those processes they calculated the cluster mass and energy changes associated with them to predict the evolution. They followed the cluster evolution only up to core collapse, and assumed a single-mass King model (King 1966) for the internal cluster structure. Tidal heating due to the GMC was found to be negligible compared to the disk shocks. Note however, that the Galactic model assumed in that work (Bahcall, Schmidt, & Soneira 1983; BSS) is strongly favorable to the disk shock for the clusters with small orbital radius since the surface density of the disk increases exponentially as the galactocentric radius decreases (see Section 2.2). Chernoff et al. (1986) has concluded that many of the clusters located within inner 3 kpc from the Galactic center have undergone core collapse, and many of them may already have been destroyed. A number of authors have pointed out that the bulge and stellar spheroid themselves could be composed of remnants of the destroyed globular clusters, if prior destruction of globular clusters occurred at high enough rate.

Another mechanism for the mass loss is the stellar evolution. Chernoff & Shapiro (1987) used a similar method to Chernoff et al. (1986) and included a power-law initial mass function for the cluster stars. Mass loss due to stellar evolution is important for the early evolution of the cluster, but then fades away because the mass loss is large only for massive stars whose lifetime is short. Comprehensive study including the effects of stellar

evolution has been done by Chernoff & Weinberg (1990). They used a Fokker-Planck code with an extensive spectrum of stellar masses (20 species), which includes stellar evolution and relaxation processes. Multi-mass models evolve much faster and the evaporation rate is larger. Also, mass segregation (Spitzer 1987) speeds up the collapse. Mass loss during first 5×10^9 yr is sufficiently strong to disrupt weakly concentrated clusters ($c < 0.6$). Combined with the relaxation, it destroys many low mass and low concentration clusters within a Hubble time.

The present characteristics and the evolutionary state of the observed Galactic globular clusters were also investigated by Aguilar, Hut, & Ostriker (1988; hereafter AHO). We will draw heavily on that paper and compare our results with AHO. AHO used a sample of the 83 Galactic globular clusters with the known structural parameters and line-of-sight velocities. They considered virtually all the important physical mechanisms (except the mass spectrum and mass loss due to stellar evolution) to calculate the present day destruction rates for the clusters in the sample. The rates were defined as the inverse time it takes for a given mechanism to dissolve a cluster, in units of a Hubble time, which is nominally defined as 10^{10} yr. They estimated the rates for the evaporation through tidal boundary, disk and bulge tidal shocks, and dynamical friction. The last process has not been widely investigated in its application for the clusters' evolution. Its effect reduces to the gradual spiraling of the cluster toward the Galactic center, as the cluster loses orbital energy due to continuous interactions with field stars and dark halo. AHO found that this mechanism is a relatively unimportant one, except for unusually massive clusters. They calculated a number of orbits associated with each cluster in the sample and took a median over the whole resulting distribution for a corresponding destruction rate. They investigated two Galactic models (OC and BSS; Section 2.2), and two kinematic models for the globular cluster system: isotropic, which corresponds to the current distribution, and predominantly radial, which resembles that of the halo stars and might be closer to an *initial* cluster distribution. The assumption concerning the velocity distribution is necessary as only one velocity component is observed. (Note however that the program to obtain the true space velocities of globular clusters is underway; see Cudworth & Hanson 1993). We will discuss the kinematic models in Section 2.3.

The central bulge was found to be very efficient in destroying clusters on a highly elongated orbits. This leads to an *isotropization* of the orbits, and even preferential survival of tangentially biased orbits in the Hubble time. Thus, an initially radial distribution better fits the present population, than the initially isotropic one. At the current time, evaporation is the most important destruction process. The difference between the two Galactic models was found to be relatively small, except for the disk shocking that obviously depends on a body of the surface mass profile. AHO introduced a weighting factor that accounts for

the fact that some orbits are less probable because of the various destruction mechanisms acting upon the cluster. Such a weighting reduces the computed rates, but converges to a similar value of 0.05 for all Galactic models and kinematic profiles considered. This implies that only 4 or 5 clusters are destroyed over a Hubble time for present conditions. But AHO treated clusters in a simplified fashion as King models and they (like other investigators) did not allow for the tidal shock relaxation phenomena. It is these defects that we remedy in the present paper.

Finally, a recent paper by Hut & Djorgovski (1992) used a statistical approach and approximate analytical estimates for the relaxation times for a sample of 140 clusters. They concluded that the current evaporation rate is $5 \pm 3 \text{ Gyr}^{-1}$ (about ten times the rate found by AHO), which means that a significant fraction of the present day clusters would be destroyed in a next Hubble time.

In this paper we make a significant improvement over AHO by applying detailed Fokker-Planck calculations to the real globular cluster sample. We describe the sample in Section 2.1 and the Galactic models in Section 2.2. Then we discuss the two kinematic models and compare the resulting properties of the orbits for our sample. In section 2.5 we describe the destruction mechanisms involved in the globular cluster evolution. We conclude section 2 with the history of our code and the formulation of the numerical strategy. Section 3 presents our results for all runs. Finally, we speculate on the possible past history and future fate of the Galactic globular clusters in Section 4. Section 5 sums up our conclusions.

2. Method

2.1. Observational Data

We have used a recent compilation of globular cluster coordinates by Djorgovski & Meylan (1993), and distances and absolute magnitudes from Djorgovski (1993). Cluster concentrations, core radii, and half-mass radii were taken from Trager, Djorgovski, & King (1993). The core-collapsed clusters were assigned a limiting concentration of $c = 2.5$. We used a constant mass-to-light ratio to obtain the cluster masses, $(M/L)_V = 3$ in solar units (Djorgovski 1993).

We selected 119 clusters out of 143 with available photometric data. All clusters in our sample have measured radial velocities which we collected from several sources. Cudworth & Hanson (1993) have derived actual space velocities for 14 clusters, but we chose not to use those data to maintain homogeneity of the sample. We assign two unknown velocity components to each cluster using our statistical method in Section 2.3.

The observed parameters of our sample are given in Table 1. The first two columns are the sequential number and cluster’s name. The next two columns are the Galactic coordinates. D is the distance in kiloparsecs of the cluster from the Sun, and R is its galactocentric radius. The seventh column is concentration $c = \log(R_t/R_c)$, followed by core radius R_c in parsecs. Tidal radius R_t was calculated from the previous two quantities. The next column is the cluster mass converted from its luminosity. The last two columns are the line-of-sight velocities and the reference numbers to the various sources. The references are listed in the comments to the Table 1.

2.2. Galactic Model

To evaluate the gravitational shocks on the clusters we have used two models for our Galaxy: the Ostriker-Caldwell (1983) model D-150 (OC), and the Bahcall, Schmidt, & Soneira model (1983; BSS). AHO present a detailed comparison between the two models. In the OC model the disk is represented as the difference of two exponentials which vanishes at the center, whereas BSS’s disk density rises monotonically as R decreases. The BSS model has also a compact nuclear component within 1 central kiloparsec. Thus both disk and bulge shocks (Section 2.5) are expected to be more prominent for BSS model. As suggested by AHO, we consider the difference of the results of the two models as a measure of the uncertainty associated with the distribution of mass within the Galaxy.

We use the same routine to compute the Galactic model as was done by AHO (the routine was kindly provided to us by L. Aguilar).

2.3. Velocity Distribution for the Globular Cluster System

Kinematic models for the Galactic Globular Cluster System (GCS) have been sought widely in the past (e.g., Frenk & White 1980; Thomas 1989). Frenk & White (1980) studied a sample of 66 clusters and found no evidence for the radial expansion of the GCS as a whole. Their best fit to the observed kinematic distribution is that with the isotropic velocity dispersion rising with the galactocentric distance as $R^{0.2}$. An isotropic and isothermal (with constant velocity dispersion) model is still consistent with their data at the 90% confidence level. Later work by Thomas (1989) included 115 clusters and confirmed the absence of the expansion. He found that within the inner 7 kpc to the Galactic center the velocity distribution is isotropic, but for the outer radii a velocity ellipsoid with slightly increasing line-of-sight velocity dispersion may be preferred. Rotation velocity estimates

and line-of-sight velocity dispersions as well as their errors for the both sources are given in Table 2.

We repeated the analysis of the velocity distribution using our sample. We adopted the solar motion relative to the LSR of $(-9, 12, 7)$ km s $^{-1}$ (Mihalas & Binney 1981), and the circular velocity of the LSR of 220 km s $^{-1}$. Line of sight projections of the two velocities were subtracted from the observed radial velocities to obtain ones relative to an inertial frame. Then the rotation velocity and its uncertainty were estimated using equations (15) and (16) of Thomas. After subtraction of the rotation velocity along the line of sight we end up with the peculiar velocities with (presumably) zero mean. Both our v_{rot} and σ_{los} are in agreement with the above results within errors. Our adopted values are also summarized in Table 2.

Following AHO we investigate two *initial* kinematic models for the globular cluster system. The first one has an isotropic peculiar velocity distribution with constant velocity dispersion. This is the simplest model still consistent with the observations. We used the one-dimensional dispersion of 118 km s $^{-1}$, resulting from our sample.

The second model is anisotropic with velocity ellipsoid axis ratio at solar position $r_{\odot} = 8.5$ kpc similar to the spheroid stellar population II:

$$\frac{\sigma_r^2}{\sigma_t^2} = 1 + \frac{r^2}{r_a^2}, \quad (1)$$

where σ_r and σ_t are the one-dimensional dispersions radial and transverse to the Galactic center, respectively. We have adopted the AHO value of the anisotropy radius $r_a = 0.8^{1/2} r_{\odot} \approx 7.6$ kpc. Cluster orbits for this distribution are nearly isotropic within r_a , and become more and more radial with increasing distance from the center.

The amplitude of the radial velocity dispersion can be obtained from Jeans equation for the constant circular velocity potential. Integrating the Jeans equation in spherical coordinates gives (e.g., Ogorodnikov 1965):

$$\frac{d\rho\sigma_r^2}{dr} + \frac{\rho}{r} (2\sigma_r^2 - 2\sigma_t^2 - v_{\text{rot}}^2) = -\rho \frac{v_{\text{circ}}^2}{r}. \quad (2)$$

For the velocity ellipsoid given by equation (1) and the power-law density profile $\rho \propto r^{-\alpha}$, we obtain

$$\sigma_r^2 = (v_{\text{circ}}^2 - v_{\text{rot}}^2) \frac{\frac{r^2}{\alpha-2} + \frac{r_a^2}{\alpha}}{r^2 + r_a^2}. \quad (3)$$

We accept $v_{\text{circ}} = 220$ km s $^{-1}$ as the standard value for the circular velocity. Thomas found $\alpha = 3.5$ for his sample of globular clusters. In this paper we assume $\alpha = 3$, corresponding to the old spheroid stellar population.

The distribution of peculiar velocities at a given galactocentric position r of a cluster is then (AHO eq. [4])

$$f(v_r, v_{t1}, v_{t2}) = A \exp \left[-\frac{v_r^2}{2\sigma_r^2} - \frac{v_{t1}^2 + v_{t2}^2}{2\sigma_t^2} \right], \quad (4)$$

where v_r is the radial galactocentric velocity, and v_{t1}, v_{t2} are the two transverse components.

The distribution of orbital eccentricities is shown in Figures 1 and 2 for the OC and BSS models, respectively. Upper panels in both figures show histograms for the anisotropic velocity ellipsoids, and the lower ones for the isotropic distribution. Note how the number of large eccentricities changes from the former to the latter.

2.4. Orbit Integration

In order to model the gravitational shock experienced by a cluster flying by the galactic center (bulge shock) we need an estimate of a perigalacticon distance R_{peri} and orbit shape (eccentricity e) for each cluster from our sample. We use the orbit integration routine described in AHO, which employs a 4th order Runge-Kutta method with variable time step. The Galactic model extends up to a distance of 250 kpc, and all orbits beyond that point are discarded.

Only 4 out of the needed 6 phase space parameters required to start the calculation of orbits are known from the observations (Table 1): 3 spatial coordinates and a velocity component along the line of sight. To complement the two “missing” tangential velocities we used a statistical approach similar to that of AHO. The two velocities were randomly drawn and then selected using the rejection method (Press et al. 1992) in order for the total three-dimensional peculiar velocity be consistent with the assumed kinematic model (section 2.3). The systemic rotation velocity was then added to the peculiar velocity, and the resulting velocity with respect to the Galactic center was used for the orbit integration.

We have followed trajectories that each cluster makes in 10 billion years. Perigalactic and apogalactic distances were calculated as medians from the set of all orbits. Similarly we determine the velocity of the cluster at the perigalacticon (which we use to calculate the amplitude of the bulge shock, section 2.5.3), and the vertical velocity component at the point where the cluster crosses the disk (to estimate the strength of the disk shock, section 2.5.2). Thus only one “mean” orbit is used to evaluate the gravitational shocks.

In contrast to AHO, we could not follow every orbit of a cluster because of the nature of the Fokker-Planck calculations. The code has the time step controlled by the

relaxation processes, and it seems hard to reconcile with the orbit integration procedure. We plan however to return to this subject in next paper and try to perform simultaneous Fokker-Planck and orbital calculations which would allow us to model the evolution of the clusters in a more natural way.

2.5. Dynamical Processes

2.5.1. Evaporation

Two-body relaxation leads to the escape of stars approaching the unbound tail of the cluster velocity distribution (Ambartsumian 1938; Spitzer 1940). Tidal truncation due to the Galactic potential accelerates this process. Much more dramatic effects result from the gravothermal instability, when the inner part of cluster contracts (core collapse), and the envelope expands. This, in turn, accelerates the rate of evaporation of stars from the cluster. A recent review of pre- and post-core-collapse evolution of a tidally truncated cluster is given by Goodman (1993).

It is conventional to express the life-time of a cluster in terms of the half-mass relaxation time (Spitzer & Hart 1971)

$$t_{\text{rh}} \equiv 0.138 \frac{M^{1/2} R_h^{3/2}}{G^{1/2} m_* \ln(\Lambda)}, \quad (5)$$

where M is the total cluster mass, R_h is the half-mass radius, m_* - average stellar mass, and $\ln(\Lambda) = \ln(0.4N)$ - Coulomb logarithm, N being the number of stars in the cluster. Hénon 1961 introduced the “escape probability”

$$\xi_e \equiv -\frac{t_{\text{rh}}}{M} \frac{dM}{dt}. \quad (6)$$

Here dM/dt is the mass-loss due to two-body relaxation. For the self-similar solutions Hénon found $\xi_e \approx 0.045$. See GLO for detailed discussions of the evaporation time scale.

2.5.2. Disk Shock

When a cluster passes through the Galactic disk, it experiences a time-varying gravitational force pulling the cluster toward the equatorial plane. The characteristic time-scale for this force is the time it takes the cluster to cross two vertical scale-heights of the disk, H :

$$t_{\text{cross}} \equiv \frac{2H}{V_z}, \quad (7)$$

and V_z is the cluster velocity component perpendicular to the Galactic plane. Because of the large orbital velocity of the cluster and the relatively small vertical extent of the disk, the crossing time is usually shorter than the orbital period of stars in the outer part of the cluster. Owing to the short-term nature of the effect, it was called a “compressive gravitational shock” (Ostriker, Spitzer, & Chevalier 1972). On average, stars gain energy and the cluster binding energy is reduced. This accelerates the escape of stars from the cluster through evaporation.

On the other hand, in the central region of the cluster the effect of the compressive shock is largely damped, since the stars move very fast and their orbits become adiabatically invariant. The impact of the shock is thus a strong function of the position of a star inside the cluster. Following Spitzer, we define an *adiabatic parameter*

$$x_d \equiv \frac{2\omega H}{V_z}, \quad (8)$$

where ω is the angular velocity of stars inside cluster (assuming for simplicity circular motions), and the subscript d stands for disk; x_d represents the ratio of the shock duration to the orbital period of a star, so that for small values of ω the term “shock” is appropriate.

To evaluate quantitatively the effect of the disk shock, several approaches have been proposed in the literature. The simplest one, the impulse approximation, assumes that the shock is so fast that the star does not change its position in the cluster significantly over the time t_{cross} . However, for the reason of adiabatic conservation, this approximation highly overestimates the impact when $x_d \gtrsim 1$. A more careful treatment is given by a harmonic potential approximation (Spitzer 1958), where we assume all stars, initially at same radial distance r from the center of the cluster, move around the center with the same oscillation frequency ω . Then, referring to the equation (25) of KO, the average energy shift for every star is

$$\langle \Delta E \rangle_{\text{disk}} = \frac{2g_m^2 r^2}{3V_z^2} A_d(x_d), \quad (9)$$

where g_m is the maximum gravitational acceleration experienced by stars due to the disk. Here $A_d(x_d)$ is the factor taking into account the adiabatic invariants. For the harmonic approximation (e.g. Spitzer, eq. [5-28])

$$A_{d1}(x) = \exp\left(-\frac{x^2}{2}\right). \quad (10)$$

We refer to equation (10) as a *Spitzer correction*. However recently Weinberg (1994) showed that small perturbations of stellar orbits can still grow in a system with more than one degree of freedom. If the system is represented as a combination of multidimensional

nonlinear oscillators, it is very likely that some of the perturbation frequencies will be commensurable with the oscillation frequencies of stars. Then those orbits receive a significant kick from the perturbation, and thus no longer conserve their actions. Averaging over whole cluster can give an appreciable change in velocity and energy. Such resonances can occur even for an arbitrary small resonant mode. Consequently, the adiabatic factor $A_d(x)$ is not exponentially small for large x , but rather a power-law. The simplest form of the correction can be written as

$$A_d(x) = \left(1 + \frac{x^2}{4}\right)^{-3/2}. \quad (11)$$

For large $x \gg 1$, $A_d \propto x^{-3}$.¹ In the following, we call equation (11) the *Weinberg correction*. Figure 3 shows the difference between the two forms of the adiabatic correction. A much more detailed discussion of the Weinberg correction can be found in Gnedin et al. (1996).

Besides the shift in energy of stars $\langle \Delta E \rangle$, a gravitational shock also induces a quadratic term $\langle \Delta E^2 \rangle$, which governs the dispersion over energy spectrum and thus pushes some loosely bound stars outside the tidal radius, speeding the disassociation of the cluster. “Shock-induced relaxation” was mentioned briefly in Spitzer & Chevalier (1973; see also Spitzer 1987, p. 116²). Recently KO noted the importance of this effect. We refer a reader to that paper, in which it is shown that this tidal shock relaxation can be in many cases competitive with two-body relaxation in causing the evolution of a cluster. Like ordinary relaxation it causes a spread (diffusion) of initially similar orbits and ultimately will tend to induce core collapse.

According to KO (their eq. [25])

$$\langle \Delta E^2 \rangle_{\text{disk}} = \frac{4 g_m^2 \omega^2 r^4}{9 V_z^2} A_{d2}(x), \quad (12)$$

where in the harmonic approximation

$$A_{d2}(x) = \frac{9}{5} \exp\left(-\frac{x^2}{2}\right). \quad (13)$$

Note that the correction in this form does not match unity for $x \ll 1$. Rather it goes a factor 1.8 over the impulse approximation. The harmonic potential obviously does not apply for the outer parts of the cluster, so some mismatch is expected. On the other hand,

¹This power law index was suggested by S. Tremaine.

²We are indebted to L. Spitzer for pointing out this reference to us.

it enhances the shock in the cluster halo. We have chosen not to modify the Spitzer’s formula, and compare the calculations with those resulting from the Weinberg correction. The latter has been used in the same form of equation (11) for both energy terms. We have performed calculations with the two forms of the adiabatic correction, and also a test case in the impulse regime (no correction was applied, $A_d \equiv 1$).

Disk shocks occur twice during the orbital period of the cluster, so we define the disk shock time scale at the half-mass radius (neglecting the adiabatic vcorrections) as

$$t_{\text{disk}} \equiv \frac{P_{\text{orb}}}{2} \left(\frac{-E}{\Delta E_h} \right) = \frac{3}{8} \left(\frac{V_z}{g_m} \right)^2 P_{\text{orb}} \omega_h^2, \quad (14)$$

where P_{orb} is the orbital period, $E \approx -0.2GM/R_h$ - cluster energy, and the ΔE and ω are evaluated at R_h . Analogously, we find that

$$t_{\text{disk},2} \equiv \frac{P_{\text{orb}}}{2} \left(\frac{E^2}{\Delta E_h^2} \right) = \frac{3}{4} t_{\text{disk}}. \quad (15)$$

Both these terms contribute to the destruction of the cluster (although by quite different processes: $\langle \Delta E \rangle$ enhances evaporation and $\langle (\Delta E)^2 \rangle$ enhances core collapse), so that the total destruction rate associated with the disk shock may be written roughly as

$$\nu_{\text{disk}} \equiv \frac{1}{t_{\text{disk}}} + \frac{1}{t_{\text{disk},2}} = \frac{7}{3} t_{\text{disk}}^{-1}. \quad (16)$$

2.5.3. Bulge Shock

Similar to the compressive disk shock, every globular cluster experiences a tidal shock during its passage close to the Galactic center. The massive compact component at the center of the Galaxy (bulge) induces a strong tidal force on the cluster near the perigalactic point of the cluster orbit. The difference between this effect and that from the smooth and steady tidal field of the Galaxy is primarily due to the time dependence of the bulge shock.

The very close effect of the tidal shock induced by giant molecular clouds was considered by L. Spitzer as early as (1958). The disturbing object was represented as a point-mass, and cluster orbit near the point of the closest approach (perigalacticon in our case) is assumed to be a straight path. Employing the harmonic approximation we find the energy change for each star due to the bulge shock:

$$\langle \Delta E \rangle_{\text{bulge}} = \frac{4}{3} \left(\frac{G M_b}{V_p R_p^2} \right)^2 r^2 A_{b1}(x_b) \chi(R_p) \lambda(R_p, R_a). \quad (17)$$

Here M_b is the bulge mass, V_p is the cluster velocity at the perigalacticon R_p , and A_b is the corresponding adiabatic correction. Two new corrections arise as follows. The distribution of the bulge mass extends up to many kiloparsecs, and for some clusters it is not a good approximation to consider the bulge as a point-mass. Rather, the tidal field exerted by such an extended mass profile will differ from the point-mass field (given by, e.g., Spitzer). Details of the calculation of the correction factor $\chi(R_p)$ allowing for that effect will be given elsewhere (Gnedin & Hernquist 1996).

We give here only the final expression which we use in our calculations:

$$\chi(R_p) = \frac{1}{2} \left[(3J_0 - J_1 - I_0)^2 + (2I_0 - I_1 - 3J_0 + J_1)^2 + I_0^2 \right], \quad (18)$$

where

$$I_0(R_p) \equiv \int_1^\infty m_b(R_p \zeta) \frac{d\zeta}{\zeta^2 (\zeta^2 - 1)^{1/2}}, \quad (19a)$$

$$I_1(R_p) \equiv \int_1^\infty \dot{m}_b(R_p \zeta) \frac{d\zeta}{\zeta^2 (\zeta^2 - 1)^{1/2}}, \quad (19b)$$

$$J_0(R_p) \equiv \int_1^\infty m_b(R_p \zeta) \frac{d\zeta}{\zeta^4 (\zeta^2 - 1)^{1/2}}, \quad (19c)$$

$$J_1(R_p) \equiv \int_1^\infty \dot{m}_b(R_p \zeta) \frac{d\zeta}{\zeta^4 (\zeta^2 - 1)^{1/2}}, \quad (19d)$$

and $m_b(R) \equiv M_b(R)/M_b$ is the normalized bulge mass distribution at radius R , with $\dot{m}_b(R) = dm_b(R)/d \ln R$.

Aguilar & White (1985; also AHO) proposed a correction of the form $\chi = 1/2 I_0^2$ only. Obviously that correction factor is everywhere smaller than our's (eq. [18]), although the difference is not dramatic. We have plotted both these factors in Figure 4. For comparison, we plot also the function $m_b(R)$, which would be the naive correction which allowed only for the mass interior radius R .

The second correction, λ , is intended to take into account the time variation of the tidal force along an elliptic orbit of a cluster. Following AHO, we take the difference of the magnitudes of the tidal force at perigalacticon and apogalacticon, as the total amplitude of the tidal effect. Thus the correction factor λ can be expressed as (AHO eq. [11])

$$\lambda(R_p, R_a) = \left[1 - \frac{M_b(R_a)}{M_b(R_p)} \left(\frac{R_p}{R_a} \right)^3 \right]^2, \quad (20)$$

where R_p and R_a are the perigalactic and apogalactic distances of the cluster, respectively.

Finally, $A_{b1}(x)$ is the corresponding adiabatic correction for the bulge shock. In the harmonic approximation we get the *Spitzer correction*: $A_b(x) = 1/2 [L_x(x) + L_y(x) + L_z(x)]$

in his notation (Spitzer 1958, eqs. [36-38]). For the *Weinberg correction* we use again the same function (eq. [11]) as for the disk shock. The argument of the A function is now different,

$$x_b = \frac{2\omega R_p}{V_p}. \quad (21)$$

Figure 5 compares the two corrections.

As in the case of the disk shock, bulge shock induces the second relaxation term

$$\langle \Delta E^2 \rangle_{\text{bulge}} = \frac{8}{9} \left(\frac{G M_b}{V_p R_p^2} \right)^2 \omega^2 r^4 A_{b2}(x_b) \chi(R_p) \lambda(R_p, R_a). \quad (22)$$

Analogously to the disk case, $A_{b2} = 9/5 A_{b1}$ in the Spitzer regime, and $A_{b2} = A_{b1}$ for the Weinberg’s one.

Similarly we define the bulge shock time scale. In this case however, the effect occurs only once per cluster orbital period.

$$t_{\text{bulge}} \equiv P_{\text{orb}} \left(\frac{-E}{\Delta E_h} \right) = \frac{3}{8} \left(\frac{V_p R_p^2}{G M_b} \right)^2 P_{\text{orb}} \omega_h^2. \quad (23)$$

$$t_{\text{bulge},2} \equiv P_{\text{orb}} \left(\frac{E^2}{\Delta E_h^2} \right) = \frac{3}{4} t_{\text{bulge}}. \quad (24)$$

Finally, total destruction rate associated with the bulge shock is

$$\nu_{\text{bulge}} \equiv \frac{1}{t_{\text{bulge}}} + \frac{1}{t_{\text{bulge},2}} = \frac{7}{3} t_{\text{bulge}}^{-1}. \quad (25)$$

2.6. Fokker-Planck code

We calculate the dynamical evolution of the globular clusters from our sample using an orbit-averaged Fokker-Planck code descended from that of Cohn (1979, 1980). The code has been modified by Lee & Ostriker (1987) and Lee, Fahlman, & Richer (1991) to include a tidal boundary and three-body binary heating. Although the code allows a multicomponent stellar mass function, we restricted ourselves in this paper to a single-component case ($m_* = 0.7 m_\odot$). This requires less parametrization of the numerical models and, we hope, gives clearer understanding of the physical processes involved. In the future, it certainly will be of interest to generalize the present calculations, including a realistic mass function. Lee & Goodman, for example, considered evaporation of a multi-mass cluster in a steady tidal field and found that the mass loss doubles compare to the single-component case.

Stars beyond the tidal boundary are not lost instantaneously, but rather follow continuous distribution function $f(E)$, as described in Lee & Ostriker (1987). This takes into account the fact that the tidal radius is not a strict “border” for the cluster, because the internal force just balances the Galactic tidal force at that point. Therefore the outer stars escape only when they go further away from the cluster. The tidal field of the Galaxy is assumed to be steady and spherically symmetric. The latter is a weakness of a one-dimensional code (for a discussion see Lee & Goodman 1995). The former assumption is valid only for a circular cluster orbit. For the actual elliptical orbit the maximum tidal stress occurs close to the perigalactic point, and probably determines the tidal cutoff radius. A theoretical estimate for R_t is given by Innanen, Harris, & Webbink (1983), who assumed a spherical mass distribution that increases linearly with galactocentric radius. However, a proper calculation of the tidal radius is still a challenge for dynamicists, including its definition itself. For our calculations we used the observed *present day* tidal radii (Table 1), which were obtained by fitting a single-mass King model to the observed cluster density profiles.

Heating of stars, reversing the core collapse, is due to three-body binaries. They are included explicitly, without following their actual formation and evolution, according to the prescription by Cohn (1985). Although Ostriker (1985) showed that the tidally captured binaries are probably more dynamically important for massive clusters than those formed through the tree-body interactions, the re-expansion phase following the core collapse is largely independent of the central heating source (Henon 1961; Goodman 1993).

2.7. Philosophy of the Numerical Experiments

Our goal in this paper is to investigate the importance of the different destruction processes on the overall evolution of the Galactic Globular Cluster System. We consider the evaporation process, and the disk and bulge gravitational shocks. AHO included also the dynamical friction in their orbit integrations, but we cannot model this effect at the moment. We rely on the AHO’s results that the dynamical friction is not an important destruction mechanism for most clusters *at the present time*.

Also, AHO evaluated the destruction rates for all of the mechanisms separately. Using the Fokker-Planck code we could investigate the effects only together, acting simultaneously. We hope this brings the numerical simulations closer to the reality, since in the real clusters all of these processes act coherently, thus “helping” each other. For example, the disk and bulge shock induced relaxation (eqs. [12,22]) combines with the normal two-body relaxation and enhances the evaporation of stars through the tidal boundary.

Nevertheless, it is of prime interest to rank the processes in their role for the destruction of the clusters. In particular, AHO found that the bulge shock is more important mechanism than the disk shock. Also the newly discovered tidal shock relaxation (KO) has never been used in the detailed calculations of globular cluster evolution. How important are these processes? We try to answer this question using a “reduction” approach. We perform several sets of runs of the Fokker-Planck code, increasing the number of the processes allowed to act upon the cluster. The magnitude of each effect can then be estimated by subtracting the results of the run without that effect from the results of the run including the effect. Since we do not expect the effects to add in a linear fashion such an estimate will only approximately determine the strength of the effect. Thus we organized the following series: 0) evaporation only; evaporation + 1) disk shock, $\langle \Delta E \rangle$ term only, no tidal shock relaxation; 2) disk shock, including the relaxation term $\langle \Delta E^2 \rangle$; 3) disk shock + bulge shock, without tidal shock relaxation; and finally 4) disk shock + bulge shock, including the relaxation. The last run includes all the processes we consider in this paper and represents the total destruction rate computed for the globular clusters.

For each set of runs we repeat the calculations three times, allowing for different adiabatic conservation factors for the shock processes (sections 2.5.2 and 2.5.3). The first run includes the Spitzer correction, the second - Weinberg correction, and the last one assumes the impulse approximation with no adiabatic correction applied.

Each run includes the Fokker-Planck simulations for all of the clusters in our sample, starting from the present time and ending with their total destruction. We use the observed concentrations and core radii of the clusters (Table 1) to model their current structure, which we approximate by a single-mass King model. The statistically assigned kinematic parameters (R_p , R_a , V_z , V_p ; section 2.4) were used to estimate the amplitude of the tidal shocks. We followed evolution of the cluster up to a late stage near total destruction when the code breaks down due to numerical difficulties in recomputation the cluster potential. The remaining mass at that point is on average 8% (but no more than 11%) of the initial cluster mass. Destruction time t_d was extrapolated using the least-squares linear fit to the last 10 integration steps. This gives a more robust estimate of t_d than just linear extrapolation from the last couple points because many clusters suffer the gravothermal instability (e.g., Goodman 1993) at the late stages of their evolution. We return to this issue in the Results section.

Given the destruction times for all the clusters in the sample, we obtain the destruction rate in units of a Hubble time

$$\nu \equiv \frac{t_{\text{Hubble}}}{t_d} = \frac{10^{10} \text{ yr}}{t_d}. \quad (26)$$

This definition agrees with the destruction rates of AHO, thus allowing a direct comparison.

Since the resulting distribution of the rates is broad and in general asymmetric around the mean, we choose to take a median $\tilde{\nu}$ of the sample as a characteristic value, in accordance with AHO. Also, a few clusters from the sample have $\nu \sim 10^3$ and therefore dominate in the mean and standard deviation. The standard error of the median was estimated as (Kendall, Stuart, & Ord 1987)

$$\sigma_{\tilde{\nu}} = \frac{1}{2 N^{1/2} f(\tilde{\nu})}, \quad (27)$$

where $f(\tilde{\nu})$ is the probability density distribution evaluated at the median point. For our sample we write $f(\tilde{\nu}) = \Delta N / N \Delta \nu$, since f should be normalized to unity. Taking $\Delta N = 0.5 N^{1/2}$, we define the two-sided errors

$$\sigma_{\tilde{\nu}}^+ = \nu(N/2 + N^{1/2}/2) - \tilde{\nu}, \quad (28a)$$

$$\sigma_{\tilde{\nu}}^- = \nu(N/2 - N^{1/2}/2) - \tilde{\nu}, \quad (28b)$$

for the sorted sample of ν .

3. Results

The results of our calculations for the individual clusters are presented in Table 3. Here we show the destruction rates for the two galactic models and the isotropic starting kinematics of the clusters (the anisotropic model is omitted for brevity). The Weinberg adiabatic correction is assumed throughout the Table. The first two columns identify the clusters and are the same as in Table 1. The third column gives the half-mass relaxation time in years. The remaining columns present the median destruction rates per Hubble time for each cluster in the sample. The first is the evaporation rate, followed by the runs including the tidal shocks: first and second order disk shock, and first order disk+bulge shocks for both the galactic models. The columns 7 and 10 give the total destruction rates corresponding to our present time globular clusters. The rest of this section discusses the statistical results for the sample.

3.1. Evaporation

We turn first to the evaporation of stars from clusters. In other words we perform a set of integrations where we allow only for ordinary two-body relaxation and losses over the tidal boundary. Although many studies have been devoted to normal two-body relaxation, we are unaware of any complete survey of a distribution of destruction times for different cluster parameters. Figure 6 shows the evaporation time in units of the initial relaxation

time versus cluster structural parameter, concentration $c = \log(R_t/R_c)$, where R_t and R_c are the tidal and core radii, respectively.

Almost all points on this Figure lie along one curve. This makes it very useful for quick estimates of the evaporation time given the initial parameters of a cluster. The least-squares fit gives

$$\frac{T_{rh}}{T_{ev}} = 1.290 \times 10^{-1} - 1.170 \times 10^{-1} c + 3.282 \times 10^{-2} c^2 + \frac{7.355 \times 10^{-4}}{(c - 0.55)^2}, \quad (29)$$

where T_{rh} is the half-mass relaxation time, and T_{ev} is the total evaporation time. Our fit is shown on Figure 6 as a solid line.

This result suggests that the loosely bound clusters, with $c < 0.65$, are destroyed very fast (in units of the relaxation time). The most stable against relaxation are the clusters with $c = 1.5 - 2$, which survive for about $40 t_{rh}$. But this number decreases to $20 t_{rh}$ as the concentration rises beyond 2. Similar behavior has been found by Johnstone (1993; his Fig. 2).

The correlation between T_{ev} and T_{rh} could be attributed to the fact that the King models (the initial condition for our calculations) belong a one-parameter family, and so can be described by the concentration parameter only. This holds only for the dimensionless quantities, such as the ratio T_{ev}/T_{rh} . The plot of the current relaxation time, expressed in years (Figure 7), does not show any obvious correlation with the concentration of the clusters.

3.2. Gravitational Shocks

Inclusion of the gravitational shocks speeds up the destruction of the clusters dramatically. Table 4 summarizes the results of our simulations when all the physical processes are acting on the clusters. The destruction rates are calculated as medians for the sample (see Section 2.7). In the OC galactic model the shocks almost double the destruction rate due to relaxation. Disk shocking (“old” first order) has little effect for both isotropic and anisotropic kinematic models, but the shock induced relaxation is more pronounced (0.09 in the median rate gain versus 0.017 in the former case). The case with the Spitzer correction is enhanced in the shock relaxation and bulge shocks because of the over-impulse increase of the adiabatic corrections (Section 2.5.2). The bulge shock is much stronger, and in the isotropic model it completely dominates over the disk shock. For the anisotropic model, the destruction associated with the bulge shock is reduced. Total destruction rate for the OC model is in the range 0.45 – 0.58.

In the BSS galactic model the disk is stronger, and there is a nuclear component that dominates the tidal shock over large range of radii (cf Figure 4). Therefore the destruction rates are significantly increased by the shocks: they range from 0.63 to 0.86.

Next, we investigate the dependence of the destruction rates on the current observed cluster position. Figure 8 shows the destruction rates associated with the several combinations of the physical mechanisms (Section 2.7) versus galactocentric radius, for the OC galactic model and isotropic kinematic model for the clusters (Section 2.3). We use here calculations with the Weinberg adiabatic correction. The left top panel, corresponding to the two-body relaxation, is largely determined by the selection of our sample, since relaxation is an internal process. However the steady increase in the rate with the decreasing distance to the galactic center is most likely explained by the growing tidal field that imposes tidal cutoff, and therefore removes stars from cluster faster. Going from the left top panel to the middle bottom we include more and more tidal shock processes. The disk in the OC model is relatively weak and does not change the distribution noticeably. Bulge shocks, on the other hand, enhance the destruction in the center considerably. Relaxation induced by the bulge shock is comparable to the first order effect. For clusters within 2 kpc of the center of the Galaxy, tidal shock relaxation dominates ordinary two-body relaxation in determining the cluster evolution. For such clusters core collapse occurs much faster and overall evolution proceeds on the shock time scale, when it is shorter than the relaxation time. During the cluster contraction, the relative importance of the tidal shock relaxation to ordinary two-body relaxation decreases and the final stage of core collapse is described by the self-similar solutions of Hénon 1961. After core collapse the cluster is still so highly concentrated that the density profile is close to an isothermal sphere. Slow expansion along with the tidal stripping of stars leads to final dissolution of the cluster.

A similar plot for the anisotropic kinematic model is given in Figure 9. Figures 10 and 11 show the distribution for the BSS galactic model and the isotropic and anisotropic kinematics, respectively.

To emphasize the relative importance of each of the destruction mechanisms, we define the *differential* rates by subtracting the destruction rates obtained without that process from the run including the process. Namely, first-order disk shock (“disk1”) is “evaporation + disk1” – “evaporation”, second order disk shock relaxation term (“disk2”) is “evaporation + disk” – “evaporation + disk1”, first order bulge shock (“bulge1”) is “evaporation + disk1 + bulge1” – “evaporation + disk1”, and the bulge relaxation is “evaporation + disk + bulge” – “evaporation + disk” – “bulge1”. Differential rates for the two Galactic and kinematic models are presented in Figures 12 – 15. For the reasons noted earlier (nonlinearity), these figures must be considered indicative but not exact.

We present the histograms of the distributions of the destruction rates in Figures 16 – 19. Arrows at the top show median of the distribution.

We should however be cautious using these differential results, since all those mechanisms act together and the final result is not a direct sum of the single processes. For example, relaxation is greatly enhanced by the tidal shock relaxation and core collapse occurs faster (in some cases clusters collapsed even when the ordinary relaxation was not enough to drive the contraction).

3.3. Vital Diagram for Globular Clusters

We do not know what was the initial distribution of globular clusters in our Galaxy. But we can imagine that they occupied some volume in a given parameter space. All the physical mechanisms considered above tend to destroy clusters with time, and thus to reduce the allowed volume. They superimpose particular boundaries which distinguish the present day clusters from those being already dissolved (or never formed). Fall & Rees (1977) considered the cluster mass versus their typical size (half-mass radius R_h) diagram. The authors included evaporation, disk shock and tidal shock heating (for the latter they assume the tidal interaction with the clusters themselves rather than with the bulge). These processes cut a triangle on the $R_h - M$ plane, containing the observed clusters pretty well. Ostriker (1975, unpublished) and Caputo & Castellani (1984) also included dynamical friction, which excludes the very massive clusters. They noted also that the strength of the destruction mechanisms vary with galactocentric radius, and therefore the allowed space depends on the position of a cluster.

We constructed such a vital diagram for the Galactic GCS using our sample and results of the computations of its evolution. All of the processes used in the simulations, as well as the dynamical friction, participate in the diagram. The vital boundary is defined in such a way, that the sum of all the destruction rates is equal to the inverse Hubble time:

$$\frac{1}{t_{\text{Hubble}}} = \frac{1}{t_{ev}} + \frac{1}{t_{sh}} + \frac{1}{t_{df}}, \quad (30)$$

where t_{ev} , t_{sh} , and t_{df} are the time-scales over which a cluster would be destroyed by the given process alone, for the evaporation, disk and bulge shock combined, and dynamical friction, respectively. Note that throughout this paper we adopted for simplicity $t_{\text{Hubble}} = 10^{10}$ yr.

According to the calculations reported in Section 3.1

$$t_{ev} \sim 30 t_{\text{rh}}, \quad (31)$$

where t_{rh} is the half-mass relaxation time (eq. [5]). We plan to perform a similar comprehensive analysis for the gravitational shocks. At present we use

$$t_{sh} = \frac{1}{\nu_{\text{disk}} + \nu_{\text{bulge}}} \quad (32)$$

Thus the shock boundary should be considered as a stronger limit.

We have not considered the effects of dynamical friction in details in this paper. Binney & Tremaine (1987) estimated the time for a cluster to lose its momentum and fall to the Galactic center (their eq. 7-26):

$$t_{df} = \frac{2.64 \times 10^{11} \text{yr}}{\ln \Lambda} \left(\frac{R}{2 \text{kpc}} \right)^2 \left(\frac{V_c}{250 \text{kms}^{-1}} \right) \left(\frac{10^6 M_{\odot}}{M} \right), \quad (33)$$

where $\ln \Lambda$ is the Coulomb logarithm, R is the *initial* galactocentric distance, V_c is the cluster circular speed, and M is its mass.

The cluster vital diagram for the OC galactic model is shown in Figures 20, 21.

The diagram for the BSS model is in Figure 22, 23.

One can see that a significant fraction of the clusters lies outside of the “surviving” boundary. This supports our conclusion that many clusters will be destroyed within the next Hubble time.

4. Discussion

Using the Fokker-Planck simulations and the sample of the globular clusters we estimated a current destruction rate per Hubble time. These results are applicable for the present day clusters evolving forward in time for the next Hubble time. On the other hand, it is of prime interest to extract any possible information regarding the past evolution of the clusters from the time of their formation up to now. We try to construct a simple model for the initial distribution of the clusters and to test it against the current destruction rate. We try then to answer the question raised in the Introduction: how many of the globular clusters may have been destroyed in the history of our Galaxy.

We will not attempt to propose a mechanism for the formation of globular clusters. An example of a possible formation scenario is given by Fall & Rees (1985). Instead, we assume a *life-time* function for the globular clusters, free of any particular assumptions. Let $t_d(t)$ be a time remaining to the total destruction of a given cluster at epoch t . We then define $f(t_d; t) dt_d$ to be the number of clusters with the destruction time in the interval

$[t_d, t_d + dt_d]$ at time t . Thus, if we treat almost all clusters as made in a short time interval at the formation of the Galaxy (an obviously gross over-simplification), then $f(t_d; 0) dt_d$ gives the initial distribution of cluster lifetimes. The normalization is

$$N(t) = \int_0^\infty f(t_d; t) dt_d, \quad (34)$$

where $N(t)$ is the number of clusters at epoch t . We would like to advance our function f in time starting from their formation, again without a detailed prescription for the evolution of the cluster sample. We simply assume that all the clusters were formed at the same time, and that this time $t_0 \approx 0$ is very small compare to the present Hubble time. Then number of clusters surviving at the time t is just the number of initial clusters with $t_d > t$. Thus we have the following relation:

$$f(t_d; t) = f(t_d + t; t_0), \quad (35)$$

where we have neglected the contribution of $t_0 \ll t$ in the first argument of the function f . We call $f(t_d; t_0) \equiv f_i(t_d)$ the initial distribution of the globular clusters. Integrated over all destruction times t_d it gives the initial number of globular clusters $N(t = t_0) \equiv N_i$ formed in our Galaxy.

We define also mean \bar{t}_d and median t_m destruction times according to

$$\bar{t}_d(t) = \frac{\int_0^\infty t_d f(t_d; t) dt_d}{\int_0^\infty f(t_d; t) dt_d} = \frac{\int_0^\infty t_d f(t_d; t) dt_d}{N(t)}, \quad (36)$$

$$\frac{1}{2} = \frac{\int_0^{t_m} f(t_d; t) dt_d}{\int_0^\infty f(t_d; t) dt_d} = \frac{\int_0^{t_m} f(t_d; t) dt_d}{N(t)}. \quad (37)$$

Now we choose two functional forms for $f_i(t_d)$, which we test against the distribution of the destruction rates obtained in Section 3. The simplest one is that with a constant mean destruction time for all clusters. It assumes an exponential form

$$f_{i1}(t_d) = C_1 e^{-\alpha t_d}. \quad (38)$$

It is easy to show that the mean and median for this distribution are

$$\bar{t}_{d1} = \frac{1}{\alpha}, \quad (39)$$

$$t_{m1} = \frac{\ln 2}{\alpha}. \quad (40)$$

Thus the mean destruction rate does not depend on time, and the evaporation of the clusters in this case is similar to radioactive decay. Given a current vital rate we can always calculate how many clusters survived from the beginning. $N(t)$ goes exponentially to zero

$$N_1(t) = \frac{C_1}{\alpha} e^{-\alpha t}. \quad (41)$$

The other function f we consider is a scale free power-law

$$f_{i2}(t_d) = C_2 t_d^{-q}. \quad (42)$$

This distribution is not strictly normalizable since the total number of clusters N_i diverges as t_0 approaches zero

$$N_2(t) = \frac{C_2}{q-1} t^{1-q}, \quad q > 1. \quad (43)$$

However we can successfully apply it to the present time. The corresponding mean and median are

$$\bar{t}_{d2}(t) = \frac{t}{q-2}, \quad q > 2, \quad (44)$$

$$t_{m2}(t) = t(2^{\frac{1}{q-1}} - 1). \quad (45)$$

Note that both these quantities are proportional to the time of observation. Thus it seems impossible to determine the initial cluster population for this distribution given the current rate. Fortunately, we can compare the *shape* of the distribution with the current profile to choose between the two distributions. In addition we note a very important difference consequent to the two hypothesized forms for the initial distribution. In the second (power law) case we should expect that $\bar{t}_d \sim t$; whenever we look, the time to destruction for the clusters that remain is of the same order as the age of the existing sample. In the first case this might occur, but it would require a coincidence between the initial typical time to destruction and the later point in time when an observer examines the system. *The most important point to be made in this paper is that the numbers in the last line of Table 4 are of order unity.* This is consistent with the power law assumption and allows the possibility of large fractional destruction.

On Figure 24 we plot a histogram of the destruction rates for our sample of 119 clusters for the OC galactic model. The dotted region gives the number of clusters per logarithmic bin in t_d . Two panels correspond to the results obtained for the isotropic kinematic model with the Spitzer and Weinberg adiabatic corrections, respectively. We use the medians for the two cases to determine the shape of the two models for the destruction rates. The dashed curve corresponds to the exponential model, and the solid line is for the power-law one. Both lines are normalized to the present number of clusters, $N(t_{\text{Hubble}})$.

Figure 25 shows the distribution for the BSS galactic model.

We see from this plot that both models are consistent with the actual distribution. However, in our view, the power-law case better represents the overall extended shape of the histogram. The exponential model is more concentrated around the median value,

and falls off very rapidly for large t_d . It predicts also much larger number of clusters in the center of the diagram than follows from the Fokker-Planck calculations. Therefore we favor the second choice, namely, the power-law distribution of the destruction times. Based on the results obtained for the OC galactic model and Weinberg adiabatic correction, power-law index is $q \approx 1.59 - 1.64$ (two limits are for the anisotropic and isotropic kinematic distributions, respectively). For the BSS model we find $q \approx 1.73 - 1.82$. Thus we conclude that the power-law model with $q = 1.6 - 1.8$ gives naturally the present distribution of the globular cluster destruction times.

From the last sentence immediately follows that the initial cluster population could have been much larger than the present one. The present day characteristics do not provide a definite number, though they do prefer this scenario. Thus it is quite possible that a very significant fraction of the original globular clusters have been already destroyed. Their remnants might constitute now the inner spherical stellar component of our Galaxy, i.e. the bulge. We note also from Figures 8 and 10 that clusters close to the Galactic centers are most heavily attacked by the bulge shock, and therefore most of the dissolved clusters could be in the very central region of the Galaxy. A strong bulge component present in the Ostriker & Caldwell galactic model could be enhanced by the input from the destroyed clusters. Note, that we do *not* require the existence of the bulge from the first days of the Galactic history in order to destroy the clusters. As follows from the power-law distribution, most of the initially formed clusters had relatively short life-times, and presumably were not very massive. Thus the main mechanism driving their dissolution could have been internal relaxation. Though, if present in some form, the central Galactic component would be very efficient in the cluster destruction. In any case the overall potential of the Galaxy is changed only very slightly if we were to imagine that all bulge and spheroid stars were put back into globular clusters with appropriate orbits. Thus even the bulge shock tidal evaporation processes would be essentially unchanged, if we were to put all stars in the quasispherical distribution back into clusters.

Observational data on stellar populations indicate that the spheroid of the Galaxy is kinematically and chemically distinct from the disk (Norris & Ryan 1991). Halo stars are old (with an age slightly exceeding our adopted Hubble time of 10^{10} yr) and metal poor. Because the density of the protogalactic gas cloud is not high enough to form stars efficiently, the oldest stars in the Galaxy are likely to have been formed in clusters perhaps not too different from the present population of globular clusters. Now we see most of the metal poor stars in the halo, which suggest that most of them could be left over from the disrupted clusters. Harris (1991) proposed two arguments against this idea: 1) orbits of the present globular clusters are more isotropically distributed than those of spheroid stars; 2) the clusters have systematically lower metallicity than the field stars, and

become more metal poor with increasing galactocentric distance R . But AHO and Lee & Goodman (1995) pointed out a possible solution for the former problem. The first of these arguments can be moderated if we consider the initial cluster distribution. AHO argued that the kinematic model better describing the current population is the isotropic one (see Section 2.3) with the orbits getting more and more radial as R increases. The destruction mechanisms are the strongest in the central few kiloparsecs, especially the bulge shock. Thus the clusters in the most elongated orbits with small perigalactic distance R_p would be destroyed first. Their remnants would populate the spheroid as we see it now, with the preferentially radial orbits of stars. Surviving clusters, on the other hand, have more isotropic orbits consistent with the observations.

To resolve the problem of metallicities, we refer to van den Bergh (1995), who found that $[\text{Fe}/\text{H}]$ correlates somewhat more strongly with perigalacticon R_p than with their current position R . Thus the metal rich clusters with smaller R_p , which would be destroyed first, would enrich the halo stellar population. Another solution comes from the observed age difference in the cluster population. The formation period could have been extended up to 2 – 5 Gyr (see references in Norris & Ryan 1991). Thus the very first low mass clusters could dissolve due to the internal relaxation, but their stars would enrich the primordial gas for the next generation of clusters. Our power-law hypothesis for the distribution of the clusters predicts that the mean (and median) destruction time is proportional to the time elapsed since the formation, so that newly formed clusters would be again most susceptible to disruption. If they were destroyed within the remaining 7 – 10 Gyr, their stars are the population II halo stars that we see in our Galaxy.

5. Conclusions

We have used the Fokker-Planck code to investigate the destruction rate of globular clusters in our Galaxy. We applied two forms of the adiabatic correction for gravitational shocks and found that the median results do not depend much of the particular form of the correction. The current destruction rate for the sample is about 0.5 – 0.9 per 10^{10} yr (depending on the Galactic and kinematic models), which implies that more than half of the *present* clusters is to be destroyed within the next Hubble time. This estimate is approximately a factor of ten higher than that obtained by AHO. There are two principal reasons for the change. First, our Fokker-Planck detailed calculations for each cluster give systematically larger rates of two body relaxation, and core collapse than did the essentially time scale arguments of AHO. Secondly, the new tidal shock relaxation process described by KO further reduces lifetimes by a significant amount.

Trying to understand the *original* population of Galactic globular clusters, we considered two possible models for the distribution of the cluster lifetimes. Both of them can be normalized to the median present destruction rate. We favor the power-law model on basis of a shape of the rate distribution as it naturally explains the fact that the current median time to destruction is comparable to the present mean cluster age and also because the predicted distribution of cluster destruction times provides a reasonable match to observations. The power-law distribution allows a much larger number of the clusters to have been formed initially than is currently observed, and allows the possibility that the debris of the early disrupted clusters might have formed the much of spheroid of our Galaxy.

Surdin (1995) has investigated the possibility of populating the stellar halo by remnants of the destroyed star cluster (open and globular). He comes to the conclusion that much larger number of low-mass ($10^3 - 10^4 M_{\odot}$) clusters than observed now is required to match the mass of the spheroid. This conforms to our result, since low mass (and hence, weakly concentrated) clusters have short lifetime. All those non-observed clusters have to be destroyed before the present time.

Finally we note that the inclusion of the mass spectrum in the Fokker-Planck models would strongly enhance the relaxation and core collapse, and ultimately speed up the dissolution of the clusters. This could also increase the destruction rate by a significant amount.

The destruction rates for the individual clusters are available electronically upon request.

We are greatly indebted to Hyung Mok Lee, who provided us with his Fokker-Planck code. We thank Luis Aguilar for sharing the orbit integration routine used by AHO. Many people contributed to the compilation of radial velocities for our sample. George Djorgovski has been an invaluable source of data tables and references. We are grateful to Taft Armandroff, Kyle Cudworth, Chris Kochanek, and Ruth Peterson for their data, and to Bruce Carney, Chigurapati Murali, Dave Lathau, and Charles Peterson for useful references. Konrad Kuijken has provided us with the vertical gravitational force due to the Galactic disk. Finally, we have benefited from the discussions with Jeremy Goodman, Lars Hernquist, Tomislav Kundić, Hyung Mok Lee, David Spergel, Lyman Spitzer, Scott Tremaine, and Martin Weinberg. Most of the calculations have been done on the SP2 supercomputer at the Maui High Performance Computing Center, which we gratefully acknowledge. This work was supported in part by NSF grant AST-9424416.

REFERENCES

- Aguilar, L., Hut, P., & Ostriker, J. P. 1988, *ApJ*, 335, 720
- Aguilar, L. A., & White, S. D. M. 1985, *ApJ*, 295, 374
- Ambartsumian, V. A. 1938, *Uch. Zap. L.G.U.*, 22, 19. English transl. in *IAU Symposium 113, Dynamics of Star Clusters*, ed. J. Goodman, & P. Hut (Dordrecht: Reidel), 521
- Armandroff, T. E., & Da Costa, G. S. 1991, *AJ*, 101, 1329
- Bahcall, J. N., Schmidt, M., & Soneira, R. M. 1983, *ApJ*, 265, 730
- Binney, J., & Tremaine, S. 1987, *Galactic Dynamics* (Princeton: Princeton Univ. Press), p. 428
- Cannon, R. D. 1993, poster paper presented at The Globular Cluster - Galaxy Connection Workshop, *ASP Conf. Ser.*, vol. 48, ed. G. H. Smith, & J. P. Brodie (San Francisco: ASP), cited by Da Costa & Armandroff (1995)
- Caputo, F., & Castellani, V. 1984, *MNRAS*, 207, 185
- Chernoff, D. F., Kochanek, C. S., & Shapiro, S. L. 1986, *ApJ*, 309, 183
- Chernoff, D. F., & Shapiro, S. L. 1987, *ApJ*, 322, 113
- Chernoff, D. F., & Weinberg, M. D. 1990, *ApJ*, 351, 121
- Cohn, H. N. 1979, *ApJ*, 234, 1036
- Cohn, H. N. 1980, *ApJ*, 242, 765
- Cohn, H. N. 1985, in *Dynamics of Star Clusters*, *IAU Symposium 113*, ed. J. Goodman, & P. Hut (Dordrecht: Reidel), 161
- Cudworth, K. M., & Hanson, R. B. 1993, *AJ*, 105, 168
- Da Costa, G. S., & Armandroff, T. E. 1995, *AJ*, 109, 2533
- Da Costa, G. S., Armandroff, T. E., & Norris, J. E. 1992, *AJ*, 104, 154
- Djorgovski, S. 1993, in *Structure and Dynamics of Globular Clusters*, *ASP Conf. Ser.*, vol. 50, ed. S. G. Djorgovski, & G. Meylan (San Francisco: ASP), 325
- Djorgovski, S., & Meylan, G. 1993, in *Structure and Dynamics of Globular Clusters*, *ASP Conf. Ser.*, vol. 50, ed. S. G. Djorgovski, & G. Meylan (San Francisco: ASP), 373

- Fall, S. M., & Rees, M. J. 1977, MNRAS, 181, 37P
- Fall, S. M., & Rees, M. J. 1985, ApJ, 298, 18
- Frenk, C. S., & White, S. D. M. 1980, MNRAS, 193, 295
- Geisler, D., Piatti, A. E., Claria, J. J., & Minniti, D. 1995, AJ, 109, 605
- Gnedin, O. Y., & Hernquist, L. 1996, in preparation
- Gnedin, O. Y., Hernquist, L., Johnston, K. V., & Ostriker, J. P. 1996, in preparation
- Gnedin, O. Y., Lee, H. M., & Ostriker, J. P. 1996, in preparation
- Goodman, J. 1993, in Structure and Dynamics of Globular Clusters, ASP Conf. Ser., vol. 50, ed. S. G. Djorgovski, & G. Meylan (San Francisco: ASP), 87
- Harris, W. E. 1991, ARA&A, 29, 543
- Hénon, M. 1961, Ann. d'Ap., 24, 369
- Hesser, J. E., Shawl, S. J., & Meyer, J. E. 1986, PASP, 98, 403
- Hut, P., & Djorgovski, S. 1992, Nature, 359, 806
- Innanen, K. A., Harris, W. E., & Webbink, R. F. 1983, AJ, 88, 338
- Johnstone, D. 1993, AJ, 105, 155
- Kendall, M. G., Stuart, A., & Ord, J. K. 1987, Kendall's Advanced Theory of Statistics, Vol. 1 (5th ed.; New York: Oxford Univ. Press), p. 330
- King, I. R. 1966, AJ, 71, 64
- Kulessa, A. S., & McDowell 1985, unpublished, cited by Kulessa, A. S., & Lynden-Bell, D. 1992, MNRAS, 255, 105
- Kundić, T., & Ostriker, J. P. 1995, ApJ, 438, 702
- Lee, H. M., & Goodman, J. 1995, ApJ, 443, 109
- Lee, H. M., & Ostriker, J. P. 1987, ApJ, 322, 123
- Lee, H. M., Fahlman, G. G., & Richer, H. B. 1991, ApJ, 366, 455

- Mihalas, D., & Binney, J. J. 1981, *Galactic Astronomy* (2nd ed.; San Francisco: Freeman), p. 400
- Norris, J. E., & Ryan, S. G. 1991, *ApJ*, 380, 403
- Ogorodnikov, K. F. 1965, *Dynamics of Stellar Systems* (Oxford: Pergamon)
- Ostriker, J. P. 1985, in *Dynamics of Star Clusters*, IAU Symposium 113, ed. J. Goodman, & P. Hut (Dordrecht: Reidel), 347
- Ostriker, J. P., & Caldwell, J. A. 1983, in *Kinematics, Dynamics and Structure of the Milky Way*, ed. W. L. H. Shuter (Dordrecht: Reidel), 249
- Ostriker, J. P., Spitzer, L. Jr., & Chevalier, R. A. 1972, *ApJ*, 176, L51
- Peterson, R. C., & Cudworth, K. M., 1994, *ApJ*, 420, 612
- Peterson, R. C., Rees, R. F., & Cudworth, K. M. 1995, *ApJ*, 443, 124
- Peterson, R. C., Seitzer, P., & Cudworth, K. M. 1989, *ApJ*, 347, 251
- Press, W. H., Teukolsky, S. A., Vetterling, W. T., & Flannery, B. P. 1992, *Numerical Recipes in C* (2nd ed.; Cambridge: Cambridge Univ. Press), p. 290
- Prior, C., & Meylan, G. 1993, in *Structure and Dynamics of Globular Clusters*, ASP Conf. Ser., vol. 50, ed. S. G. Djorgovski, & G. Meylan (San Francisco: ASP), 357
- Schweitzer, A. E., Cudworth, K. M., & Majewski, S. R. 1993, in *The Globular Cluster - Galaxy Connection*, ASP Conf. Ser., vol. 48, ed. G. H. Smith, & J. P. Brodie (San Francisco: ASP), 113
- Spitzer, L. Jr. 1940, *MNRAS*, 100, 397
- Spitzer, L. Jr. 1958, *ApJ*, 127, 17
- Spitzer, L. Jr. 1987, *Dynamical Evolution of Globular Clusters* (Princeton: Princeton Univ. Press)
- Spitzer, L. Jr., & Chevalier, R. A. 1973, *ApJ*, 183, 565
- Spitzer, L. Jr., & Hart, M. H. 1971, *ApJ*, 164, 399
- Suntzeff, N., Olszewski, E. W., & Stetson, P. B. 1985, *AJ*, 90, 481
- Surdin, V. G. 1995, *Astron. Lett.*, 21, 508

Thomas, P. 1989, MNRAS, 238, 1319

Trager, S. C., Djorgovski S., & King, I. R. 1993, in Structure and Dynamics of Globular Clusters, ASP Conf. Ser., vol. 50, ed. S. G. Djorgovski, & G. Meylan (San Francisco: ASP), 347

van den Bergh, S. 1995, AJ, 110, 1171

Webbink, R. F. 1981, ApJS, 45, 259

Weinberg, M. D. 1994, AJ, 108, 1398; 1403; 1414

White, S. D. M., & Frenk, C. S. 1983, in Kinematics, Dynamics and Structure of the Milky Way, ed. W. L. H. Shuter (Dordrecht: Reidel), 343

Zaritsky, D., Olszewski, E. W., Schommer, R. A., Peterson, R. C., & Aaronson, M. 1989, ApJ, 345, 759

Zinn, R., & West, M. J. 1984, ApJS, 55, 45

FIGURE CAPTIONS

Fig. 1.— Histogram of the orbit eccentricity distribution in the OC galactic model, for the isotropic and anisotropic kinematic models.

Fig. 2.— Histogram of the orbit eccentricity distribution in the BSS galactic model, for the isotropic and anisotropic kinematic models.

Fig. 3.— Comparison of the Spitzer [eq. (10)] and Weinberg [eq. (11)] adiabatic corrections for the disk shock, i. e., reductions in the energy change due to the shock because of the conservation of adiabatic invariants of stellar orbits inside the clusters, versus adiabatic parameter [eq. (8)].

Fig. 4.— Correction factors versus perigalactic distance for the bulge shock energy change due to the extended mass distribution for the bulge. Our correction [eq. (18)] is shown by solid curve, and that from Aguilar & White (1985), and subsequently AHO, is given by dots. Triangles show the normalized bulge mass profile for comparison. If the bulge were treated as a point mass, that would have been the factor.

Fig. 5.— Same as Figure 3, but for the bulge shock. The adiabatic parameter is given by equation (21).

Fig. 6.— Evaporation time in units of initial relaxation time versus cluster concentration. Dots are results of the Fokker-Planck calculations with the observational data as input. Solid line - our fit, equation (29).

Fig. 7.— Relaxation time at the half-mass radius versus cluster concentration for our sample of globular clusters.

Fig. 8.— Mean probability per Hubble time for cluster destruction due to evaporation, and the evaporation plus gravitational shocks: disk shock without relaxation, disk shock including relaxation term, disk+bulge shocks without relaxation, and disk+bulge shock including relaxation, as a function of present day galactocentric distance. The error bars indicate the interquartile range of the distribution. Weinberg adiabatic corrections are used. Galactic model is OC, and kinematic model is isotropic.

Fig. 9.— Same as Figure 8, but for the anisotropic kinematic model.

Fig. 10.— Same as Figure 8, but for the BSS galactic model.

Fig. 11.— Same as Figure 9, but for the BSS galactic model.

Fig. 12.— Differential destruction rate for different processes: evaporation, disk shock with and without induced relaxation (“disk1” and “disk”, respectively), and bulge shock with and without relaxation term (“bulge1” and “bulge”). See text for the definition of the differential rate. The error bars indicate the interquartile range of the distribution. Weinberg adiabatic corrections are used. Galactic model is OC, and kinematic model is isotropic.

Fig. 13.— Same as Figure 12, but for the anisotropic kinematic model.

Fig. 14.— Same as Figure 12, but for the BSS galactic model.

Fig. 15.— Same as Figure 13, but for the BSS galactic model.

Fig. 16.— Histogram distribution of the destruction rates from Figure 8. Weinberg adiabatic correction is used. Galactic model is OC, and kinematic model is isotropic.

Fig. 17.— Histogram distribution of the destruction rates from Figure 9. Weinberg adiabatic correction is used. Galactic model is OC, and kinematic model is anisotropic.

Fig. 18.— Histogram distribution of the destruction rates from Figure 10. Weinberg adiabatic correction is used. Galactic model is BSS, and kinematic model is isotropic.

Fig. 19.— Histogram distribution of the destruction rates from Figure 11. Weinberg adiabatic correction is used. Galactic model is BSS, and kinematic model is anisotropic.

Fig. 20.— Vital diagram for the Galactic globular clusters. Mass-radius plane is restricted by three destructing processes: relaxation, tidal shocks, and dynamical friction. Galactic model is OC, and the kinematic model is isotropic.

Fig. 21.— Same as Figure 20, but for the anisotropic kinematic model.

Fig. 22.— Same as Figure 20, but for the BSS galactic model.

Fig. 23.— Same as Figure 21, but for the BSS galactic model.

Fig. 24.— Distribution of the destruction times for our sample for the OC galactic model. All destruction processes are included. Solid line - power-law distribution, normalized to the present time, dashes - normalized exponential model.

Fig. 25.— Same as Figure 24, but for the BSS galactic model.

Table 2. Kinematic parameters of Galactic Globular Cluster System

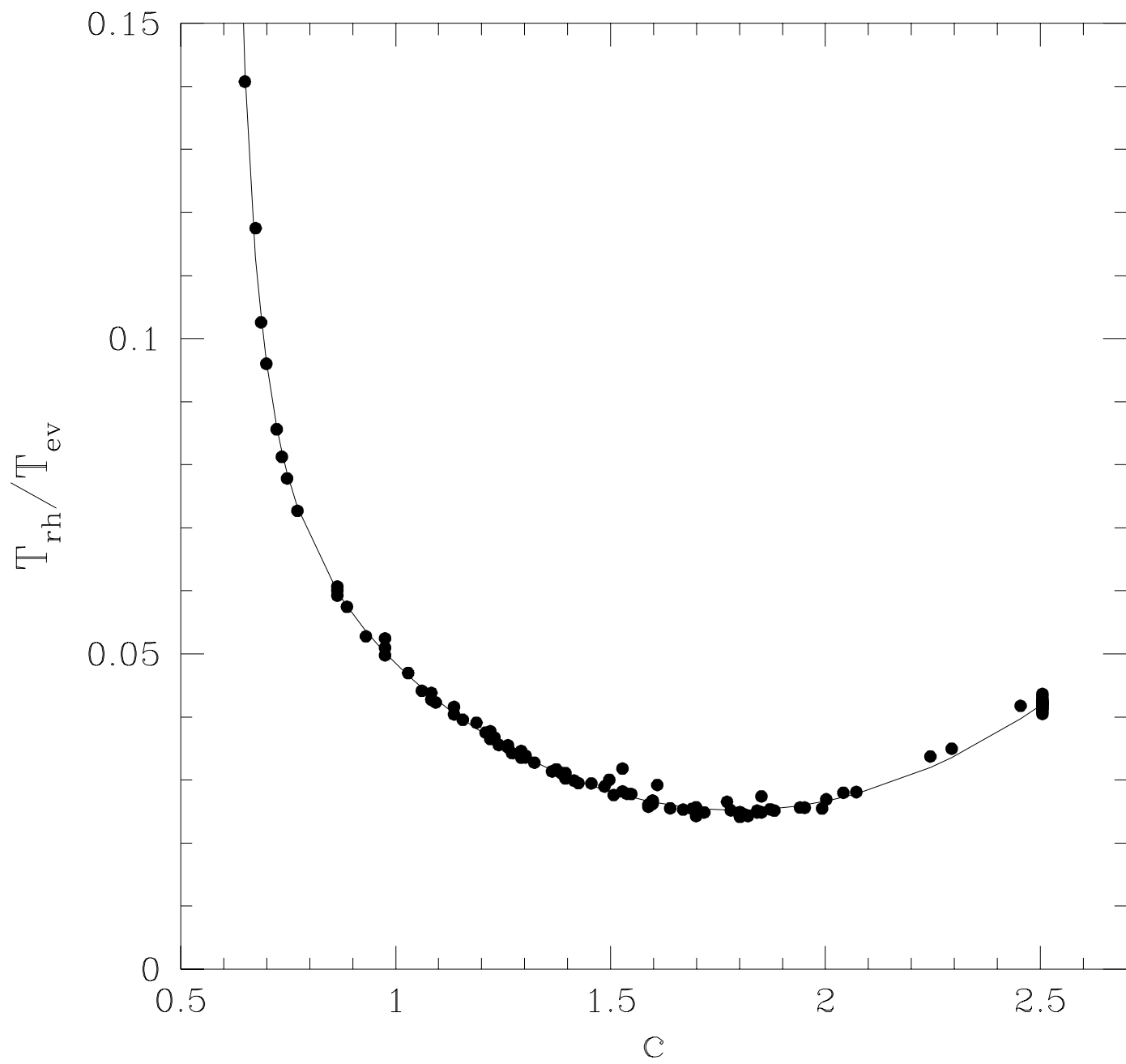
Reference	v_{rot} (km s ⁻¹)	σ_{los} (km s ⁻¹)
Frenk & White (1980)	60 ± 26	$118 \pm 20^{\text{a}}$
Thomas (1989)	65 ± 18	110 ± 7
This paper	60 ± 21	119 ± 39

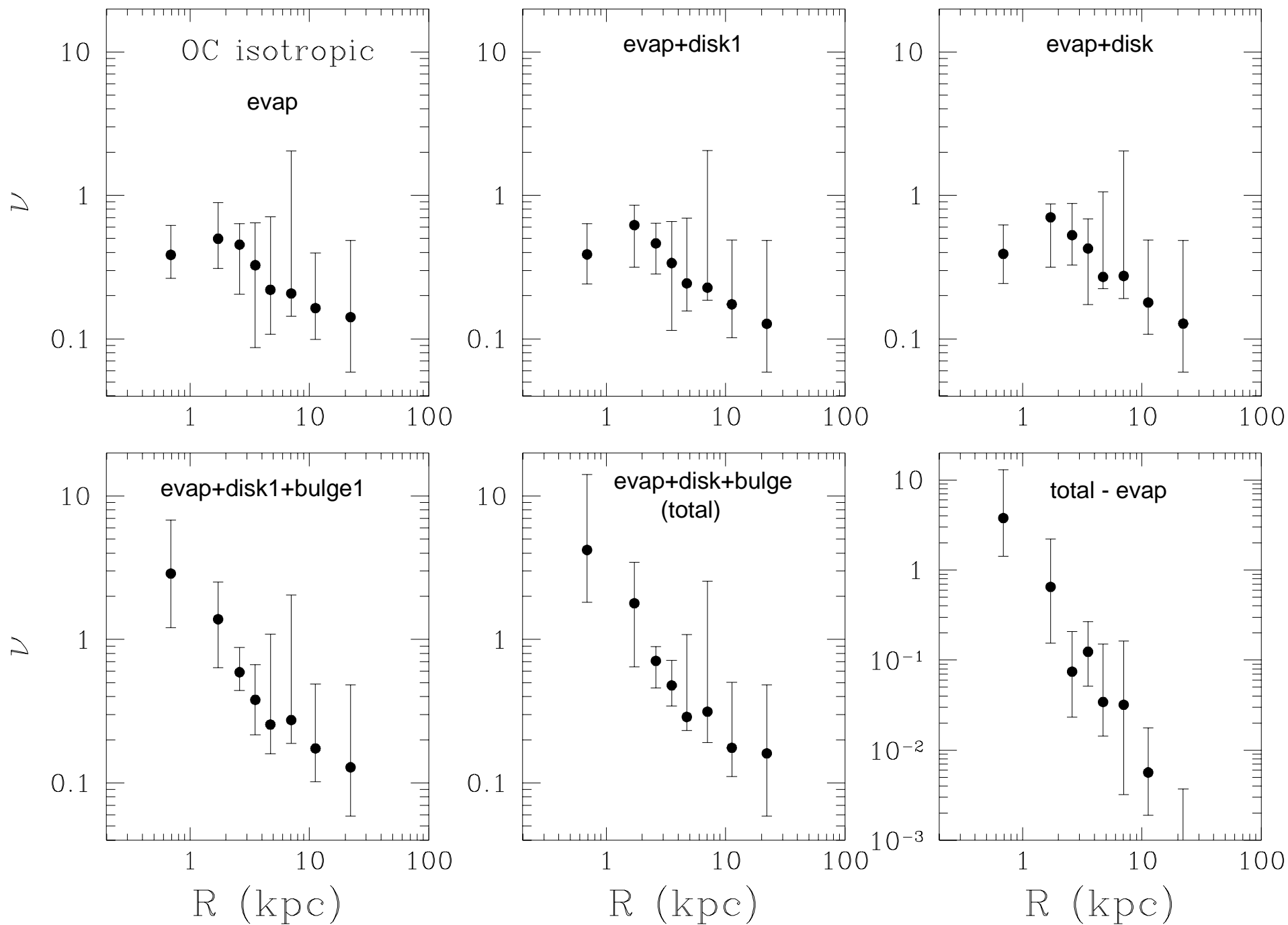
^aThe uncertainty of the velocity dispersion is taken as an average over radial bins of Table 1 from White & Frenk (1983).

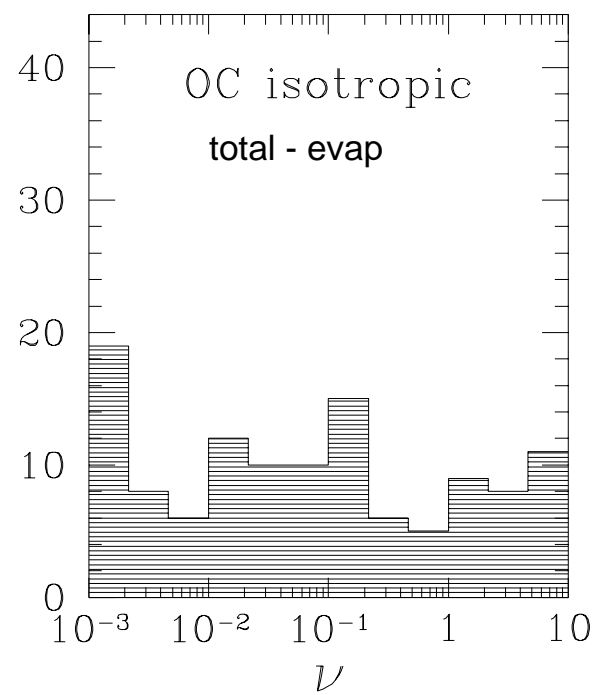
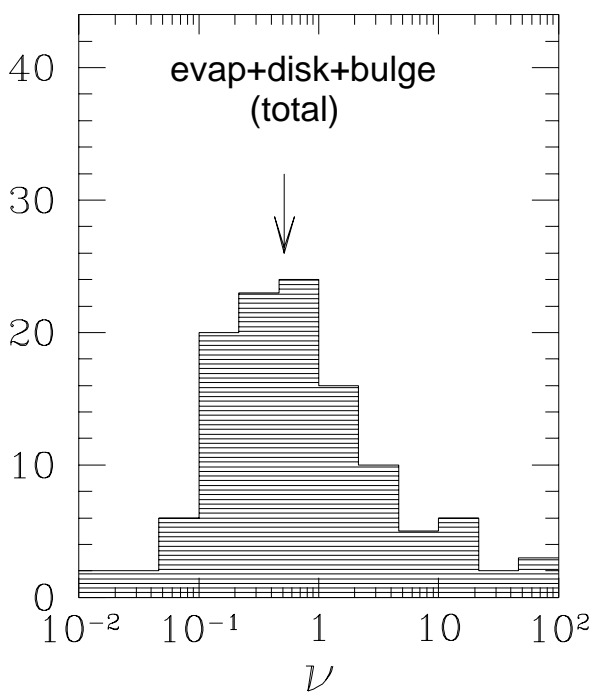
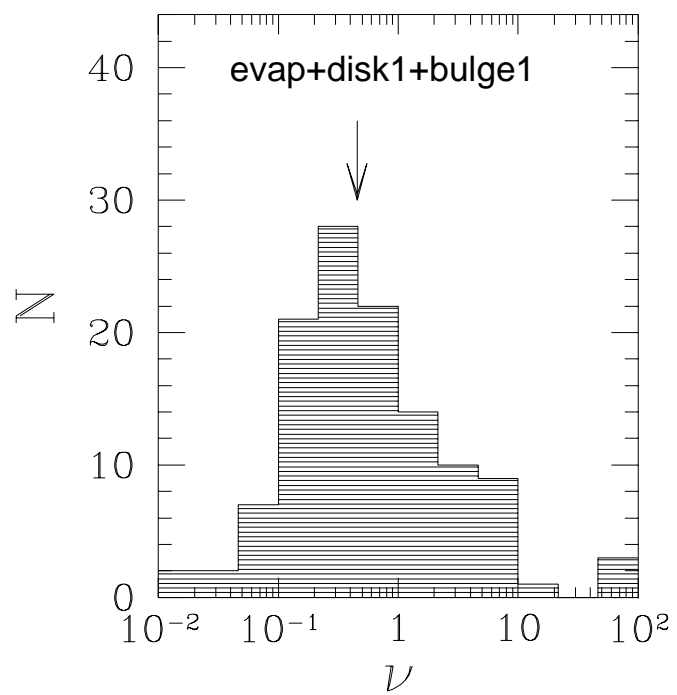
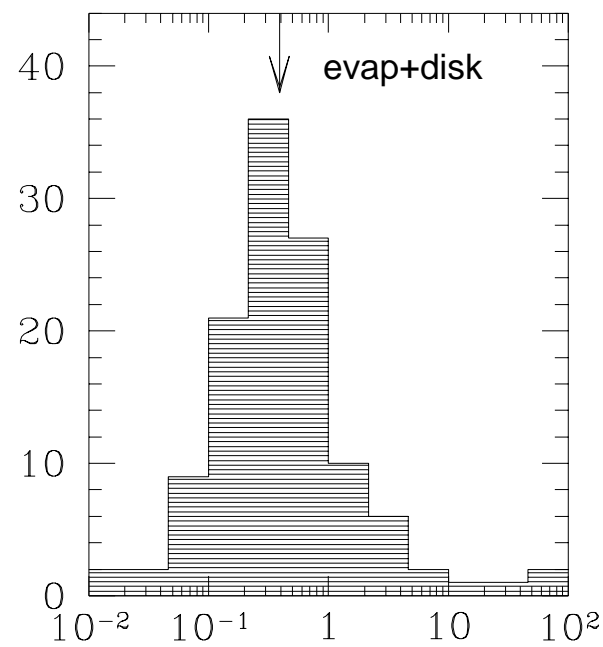
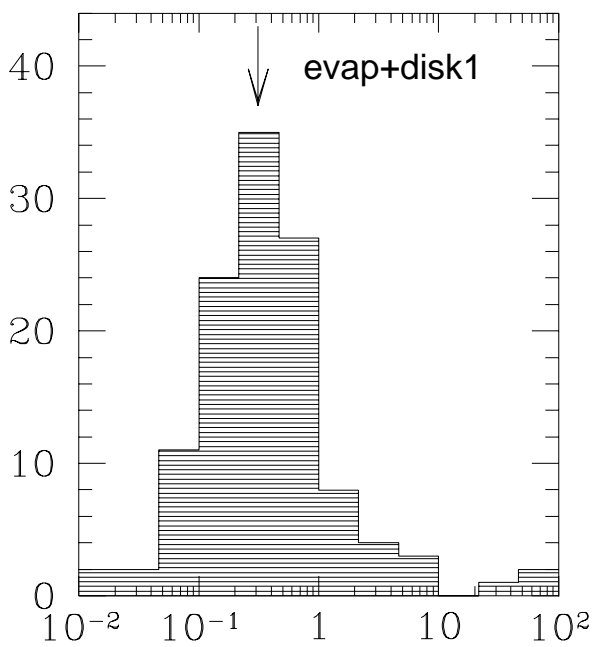
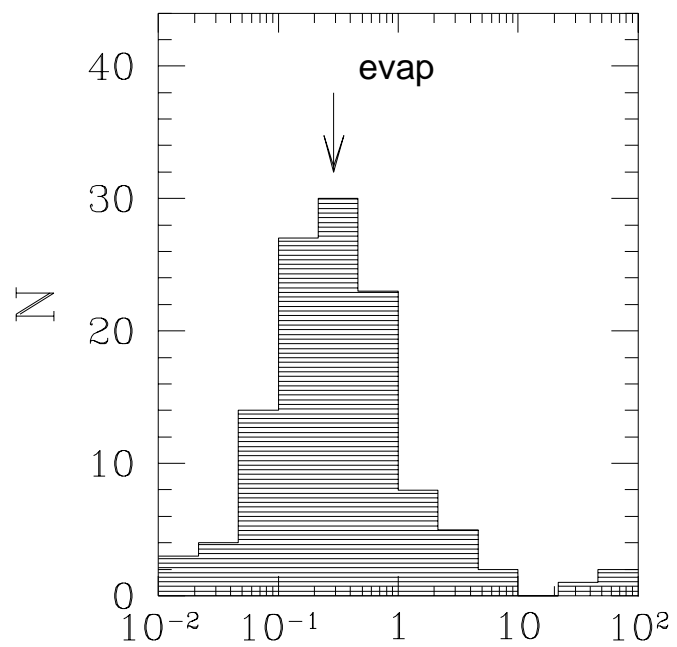
Table 4. Median Destruction Rates

Destruction Process	Isotropic			Anisotropic	
	Spitzer	Weinberg	No correction	Spitzer	Weinberg
Ostriker & Caldwell model					
Evaporation	0.290 ^{+0.020} _{-0.013}				
+ Disk 1st	0.307 ^{+0.073} _{-0.017}	0.311 ^{+0.069} _{-0.026}	0.312 ^{+0.069} _{-0.021}	0.307 ^{+0.073} _{-0.018}	0.309 ^{+0.065} _{-0.017}
+ Disk	0.397 ^{+0.021} _{-0.086}	0.391 ^{+0.012} _{-0.080}	0.394 ^{+0.011} _{-0.049}	0.393 ^{+0.021} _{-0.074}	0.365 ^{+0.033} _{-0.049}
+ Disk 1st + Bulge 1st	0.467 ^{+0.073} _{-0.058}	0.455 ^{+0.074} _{-0.059}	0.601 ^{+0.096} _{-0.091}	0.398 ^{+0.088} _{-0.085}	0.397 ^{+0.075} _{-0.077}
+ Disk + Bulge	0.583 ^{+0.133} _{-0.053}	0.518 ^{+0.108} _{-0.039}	0.905 ^{+0.048} _{-0.183}	0.490 ^{+0.138} _{-0.091}	0.453 ^{+0.116} _{-0.056}
Bahcall, Schmidt & Soneira model					
Evaporation	0.290 ^{+0.020} _{-0.013}				
+ Disk 1st	0.495 ^{+0.053} _{-0.088}	0.498 ^{+0.081} _{-0.075}	0.502 ^{+0.118} _{-0.027}	0.395 ^{+0.059} _{-0.057}	0.395 ^{+0.066} _{-0.049}
+ Disk	0.654 ^{+0.077} _{-0.101}	0.660 ^{+0.053} _{-0.124}	0.818 ^{+0.072} _{-0.159}	0.511 ^{+0.117} _{-0.045}	0.493 ^{+0.054} _{-0.058}
+ Disk 1st + Bulge 1st	0.627 ^{+0.164} _{-0.130}	0.628 ^{+0.171} _{-0.145}	1.026 ^{+0.383} _{-0.233}	0.520 ^{+0.061} _{-0.054}	0.480 ^{+0.057} _{-0.069}
+ Disk + Bulge	0.863 ^{+0.163} _{-0.181}	0.752 ^{+0.276} _{-0.110}	1.786 ^{+0.747} _{-0.699}	0.712 ^{+0.103} _{-0.061}	0.633 ^{+0.072} _{-0.053}

Note. — Rates are in fraction of sample per Hubble time (10^{10} yr). Total number of clusters in sample: 119.







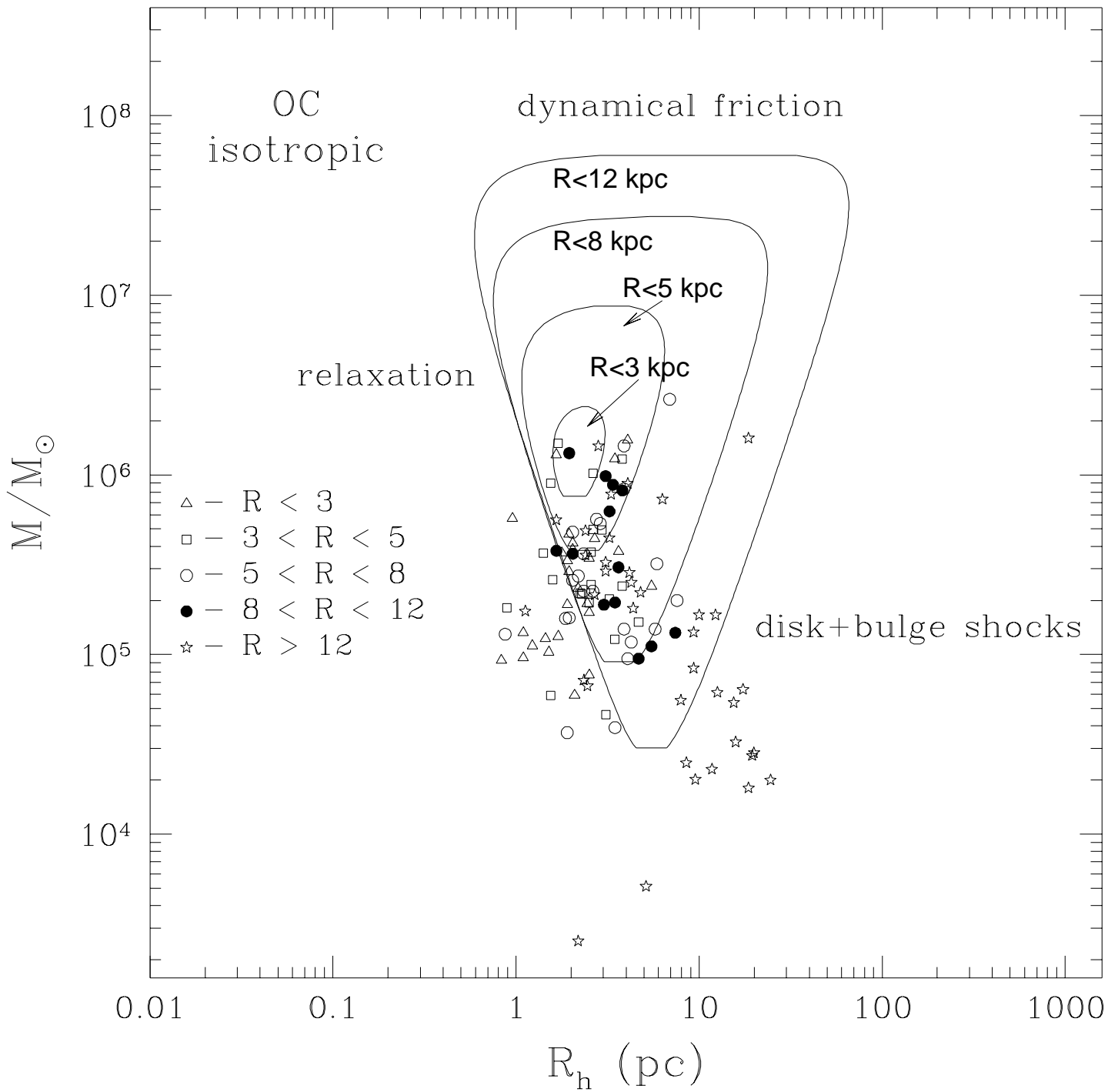


TABLE 1
GLOBULAR CLUSTER PARAMETERS

ID	Name	l (deg)	b (deg)	D (kpc)	R (kpc)	c	R_c (pc)	R_t (pc)	M (M_{\odot})	V_r (km s^{-1})	Ref
1	NGC0104	305.90	-44.89	4.6	7.8	2.04	0.50	54.8	1.45e+06	-19.0	1
2	NGC0288	152.28	-89.38	8.3	11.9	0.96	3.47	31.6	1.11e+05	-46.0	1
3	NGC0362	301.53	-46.25	8.5	9.6	1.94	0.43	37.5	3.78e+05	223.2	1
4	NGC1261	270.54	-52.13	15.9	18.0	1.27	1.82	33.9	3.26e+05	51.0	9
5	Pal1	130.07	19.03	13.7	20.1	1.50	0.60	19.0	2.54e+03	3.0	9
6	AM1	258.36	-48.47	124.7	126.1	1.23	4.57	77.6	1.81e+04	116.0	11
7	Eridanus	218.11	-41.33	79.5	84.8	1.10	5.89	74.2	2.30e+04	-21.0	10
8	Pal2	170.53	-9.07	13.6	21.9	1.40	0.60	15.1	1.74e+05	-133.0	9
9	NGC1851	244.51	-35.04	12.3	17.3	2.24	0.28	48.7	5.61e+05	320.5	1
10	NGC1904	227.23	-29.35	12.9	19.2	1.72	0.60	31.5	3.57e+05	203.4	1
11	NGC2298	245.63	-16.01	10.0	15.5	1.28	1.00	19.1	7.20e+04	150.4	3
12	NGC2419	180.37	25.24	83.2	91.0	1.40	8.51	213.8	1.60e+06	-20.0	1
13	NGC2808	282.19	-11.25	9.1	11.1	1.77	0.71	41.8	1.32e+06	98.0	9
14	Pal3	240.14	41.86	90.3	93.8	1.00	12.59	125.9	6.38e+04	84.0	9
15	NGC3201	277.23	8.64	5.1	9.3	1.31	2.09	42.7	1.95e+05	494.6	1
16	Pal4	202.31	71.80	98.2	101.0	0.78	15.85	95.5	5.41e+04	75.0	9
17	NGC4147	252.85	77.19	18.7	21.0	1.80	0.55	34.7	6.69e+04	183.0	1
18	NGC4372	300.99	-9.88	5.2	7.4	1.30	2.63	52.5	3.20e+05	49.0	9
19	Rup106	300.89	11.67	19.7	17.1	0.70	5.75	28.8	8.42e+04	-44.0	7
20	NGC4590	299.63	36.05	9.3	9.8	1.64	1.86	81.2	3.06e+05	-95.1	1
21	NGC4833	303.61	-8.01	5.8	7.2	1.25	1.70	30.2	9.49e+04	194.0	9
22	NGC5024	332.96	79.77	18.5	19.1	1.78	2.00	120.5	7.33e+05	-80.0	9
23	NGC5053	335.69	78.94	16.1	16.9	0.82	10.47	69.2	1.66e+05	42.8	1
24	NGC5139	309.10	14.97	4.9	6.8	1.24	3.72	64.6	2.64e+06	232.2	1
25	NGC5272	42.21	78.71	10.2	12.3	1.85	1.48	104.8	7.82e+05	-146.7	1
26	NGC5286	311.61	10.57	9.3	7.4	1.46	0.78	22.5	4.80e+05	57.1	1
27	NGC5466	42.15	73.59	15.8	16.3	1.43	8.91	239.8	1.33e+05	107.2	1
28	NGC5634	342.21	49.26	25.1	20.9	1.60	1.51	60.1	2.86e+05	-41.9	9
29	NGC5694	331.06	30.36	32.8	27.0	1.84	0.59	40.8	2.92e+05	-142.8	1
30	IC4499	307.35	-20.47	18.9	15.7	1.11	5.37	69.2	1.66e+05	41.0	6
31	NGC5824	332.56	22.07	32.7	26.2	2.45	0.52	146.6	8.98e+05	-26.1	1
32	Pal5	0.85	45.86	23.1	18.3	0.74	19.50	107.2	2.84e+04	-56.0	16
33	NGC5897	342.95	30.29	12.5	7.3	0.79	7.24	44.6	2.00e+05	102.9	3
34	NGC5904	3.86	46.80	7.5	6.5	1.87	0.89	66.0	8.34e+05	53.9	1
35	NGC5927	326.60	4.86	8.0	4.8	1.60	0.98	39.0	3.71e+05	-106.0	9
36	NGC5946	327.58	4.19	10.4	5.6	2.50	0.23	72.7	5.66e+05	129.0	1
37	NGC5986	337.02	13.27	10.2	4.6	1.22	1.91	31.7	4.98e+05	94.0	9
38	Pal14	28.75	42.18	73.0	67.7	0.72	23.44	123.0	2.00e+04	72.0	10
39	NGC6093	352.67	19.46	8.5	3.1	1.95	0.36	32.1	3.67e+05	7.7	1
40	NGC6101	317.75	-15.82	14.9	10.7	0.80	5.01	31.6	1.32e+05	364.3	3
41	NGC6121	350.97	15.97	2.0	6.6	1.59	0.49	19.1	2.25e+05	70.9	14
42	NGC6144	351.93	15.70	9.9	3.2	1.30	2.69	53.7	1.52e+05	162.0	9
43	NGC6139	342.37	6.94	9.1	3.0	1.80	0.35	22.1	4.18e+05	4.0	9
44	NGC6171	3.37	23.01	6.4	3.6	1.51	1.00	32.4	2.04e+05	-34.0	1
45	NGC6205	59.01	40.91	7.1	8.7	1.49	1.82	56.2	6.27e+05	-246.4	1
46	NGC6218	15.72	26.31	5.5	4.7	1.38	1.07	25.7	4.93e+05	-42.6	1
47	NGC6229	73.64	40.31	31.6	30.9	1.61	1.23	50.1	4.46e+05	-154.2	8
48	NGC6235	358.92	13.52	9.6	2.4	1.33	1.00	21.4	1.71e+05	86.0	9

TABLE 1—*Continued*

ID	Name	l (deg)	b (deg)	D (kpc)	R (kpc)	c	R_c (pc)	R_t (pc)	M (M_\odot)	V_r (km s $^{-1}$)	Ref
49	NGC6254	15.14	23.08	4.3	5.1	1.40	1.07	26.9	2.25e+05	75.5	1
50	NGC6256	347.79	3.31	10.2	2.7	2.50	0.07	22.1	7.68e+04	-104.7	1
51	Pal15	18.87	24.30	41.3	34.2	0.60	14.45	57.5	2.74e+04	68.9	1
52	NGC6266	353.57	7.32	5.6	3.1	1.70	0.29	14.5	8.98e+05	-71.9	1
53	NGC6273	356.87	9.38	10.9	2.9	1.53	1.35	45.7	1.56e+06	131.0	9
54	NGC6284	358.35	9.94	11.8	3.8	2.50	0.25	79.1	2.17e+05	27.4	1
55	NGC6287	0.13	11.02	6.7	2.3	1.60	0.52	20.7	1.03e+05	-208.0	9
56	NGC6293	357.62	7.83	8.4	1.2	2.50	0.11	34.8	2.34e+05	-148.0	1
57	NGC6304	355.83	5.38	6.0	2.7	1.80	0.36	22.7	1.93e+05	-98.0	8
58	NGC6316	357.18	5.76	12.8	4.5	1.55	0.62	22.0	1.02e+06	76.0	9
59	NGC6325	0.97	8.00	6.0	2.7	2.50	0.05	15.8	9.57e+04	30.9	1
60	NGC6341	68.34	34.86	7.5	9.5	1.81	0.51	32.9	3.64e+05	-120.5	8
61	NGC6333	5.54	10.71	7.4	2.0	1.15	1.26	17.8	2.89e+05	224.7	8
62	NGC6342	4.90	9.72	12.1	4.1	2.50	0.16	50.6	1.95e+05	117.9	1
63	NGC6356	6.72	10.22	16.6	8.5	1.54	1.12	38.8	8.19e+05	31.6	8
64	NGC6355	359.58	5.43	7.0	1.7	2.50	0.10	31.6	3.67e+05	-184.0	9
65	NGC6352	341.42	-7.17	6.1	3.5	1.10	1.48	18.6	1.22e+05	-118.0	9
66	NGC6366	18.41	16.04	4.0	5.1	0.92	2.14	17.8	3.92e+04	-122.6	1
67	NGC6362	325.56	-17.57	7.8	5.4	1.10	2.95	37.1	1.17e+05	-13.3	1
68	NGC6388	345.56	-6.74	11.0	3.7	1.70	0.40	20.0	1.50e+06	77.0	9
69	NGC6402	21.32	14.80	10.1	4.4	1.60	2.45	97.5	1.23e+06	-123.4	8
70	NGC6401	3.45	3.98	6.3	2.3	1.69	0.45	22.0	1.23e+06	-62.0	9
71	NGC6397	338.17	-11.96	2.2	6.5	2.50	0.03	9.5	1.59e+05	17.7	1
72	NGC6426	28.09	16.23	17.5	11.3	1.70	1.35	67.7	9.49e+04	-162.0	9
73	NGC6440	7.73	3.80	7.1	1.8	1.70	0.26	13.0	5.72e+05	-83.0	9
74	NGC6441	353.53	-5.00	10.7	2.5	1.85	0.35	24.8	1.30e+06	16.0	1
75	NGC6453	355.72	-3.87	10.1	1.8	2.50	0.20	63.2	1.32e+05	-84.0	9
76	NGC6496	348.02	-10.01	5.8	3.3	0.70	1.74	8.7	4.63e+04	-95.0	9
77	NGC6517	19.23	6.76	6.1	3.5	1.82	0.11	7.3	1.82e+05	-37.0	9
78	NGC6522	1.02	-3.93	7.2	1.4	2.50	0.11	34.8	5.93e+04	-10.4	1
79	NGC6535	27.18	10.44	7.0	4.1	1.30	0.83	16.6	5.93e+04	-215.3	1
80	NGC6528	1.14	-4.17	6.6	2.0	2.29	0.17	33.1	9.31e+04	160.0	9
81	NGC6539	20.80	6.78	4.0	5.0	1.60	0.63	25.1	1.60e+05	-52.0	9
82	NGC6544	5.84	-2.20	2.6	5.9	2.50	0.03	9.5	1.30e+05	-12.0	8
83	NGC6541	349.29	-11.18	6.7	2.7	2.00	0.58	58.0	4.67e+05	-152.8	8
84	NGC6553	5.25	-3.02	3.6	4.9	1.17	0.56	8.3	2.61e+05	-24.0	9
85	NGC6558	0.20	-6.03	8.9	1.0	2.50	0.09	28.5	2.41e+05	-198.9	1
86	NGC6569	0.48	-6.68	8.8	1.0	1.27	0.95	17.7	3.85e+05	-26.0	9
87	NGC6584	342.14	-16.41	9.5	3.9	1.20	1.66	26.3	2.19e+05	180.0	8
88	NGC6624	2.79	-7.91	8.1	1.3	2.50	0.15	47.4	3.32e+05	54.2	1
89	NGC6626	7.80	-5.58	6.0	2.8	1.67	0.42	19.6	4.42e+05	15.5	1
90	NGC6638	7.90	-7.15	8.4	1.6	1.40	0.65	16.3	1.12e+05	-14.0	8
91	NGC6637	1.72	-10.27	10.2	2.4	1.39	1.00	24.5	3.44e+05	50.1	8
92	NGC6642	9.81	-6.44	7.9	1.8	1.99	0.24	23.5	1.26e+05	-47.0	9
93	NGC6652	1.53	-11.38	14.3	6.2	1.80	0.30	18.9	2.59e+05	-124.2	8
94	NGC6656	9.89	-7.55	3.0	5.6	1.31	1.23	25.1	5.36e+05	-148.8	13
95	Pal8	14.11	-6.80	28.6	20.6	0.75	3.31	18.6	2.21e+05	-38.0	15
96	NGC6681	2.85	-12.51	9.2	2.1	2.50	0.07	22.1	1.89e+05	221.1	1

TABLE 1—*Continued*

ID	Name	l (deg)	b (deg)	D (kpc)	R (kpc)	c	R_c (pc)	R_t (pc)	M (M_\odot)	V_r (km s^{-1})	Ref
97	NGC6712	25.35	-4.32	6.8	3.8	0.90	1.86	14.8	2.45e+05	-107.5	1
98	NGC6715	5.61	-14.09	21.1	13.1	1.84	0.66	45.7	1.45e+06	142.0	3
99	NGC6717	12.88	-10.90	7.3	2.6	2.07	0.18	21.1	1.23e+05	-6.0	9
100	NGC6723	0.07	-17.30	8.6	2.6	1.05	2.40	26.9	3.74e+05	-79.0	9
101	NGC6752	336.50	-25.63	4.2	5.5	2.50	0.21	66.4	3.64e+05	-32.1	1
102	NGC6760	36.11	-3.92	6.1	5.1	1.59	0.59	23.0	1.38e+05	-28.0	9
103	Terzan7	3.39	-20.07	36.7	28.9	1.08	6.46	77.7	6.15e+04	162.0	2
104	NGC6779	62.66	8.34	9.7	9.6	1.37	1.05	24.6	1.89e+05	-135.9	1
105	Arp2	8.55	-20.79	28.2	20.6	0.90	13.18	104.7	3.26e+04	119.0	2
106	NGC6809	8.79	-23.27	4.8	4.6	0.76	3.98	22.9	2.41e+05	175.5	1
107	Terzan8	5.76	-24.56	23.0	15.7	0.60	6.61	26.3	2.50e+04	130.0	2
108	Pal11	31.80	-15.58	13.2	7.9	0.69	7.76	38.0	1.38e+05	-68.0	8
109	NGC6838	56.74	-4.56	3.9	7.2	1.15	0.72	10.2	3.67e+04	-23.0	1
110	NGC6864	20.30	-25.75	18.7	12.4	1.88	0.51	38.7	4.89e+05	-195.2	8
111	NGC6934	52.10	-18.89	14.8	12.0	1.53	1.07	36.3	2.15e+05	-412.2	1
112	NGC6981	35.16	-32.68	18.1	13.7	1.23	2.82	47.9	1.81e+05	-309.0	9
113	NGC7006	63.77	-19.41	38.8	36.1	1.42	2.75	72.3	2.52e+05	-364.0	9
114	NGC7078	65.01	-27.31	10.4	10.7	2.50	0.21	66.4	9.84e+05	-107.1	12
115	NGC7089	53.38	-35.78	11.8	10.7	1.80	1.17	73.8	8.81e+05	-3.1	1
116	NGC7099	27.18	-46.84	7.4	7.1	2.50	0.12	37.9	2.74e+05	-185.7	1
117	Pal12	30.51	-47.68	19.1	15.8	0.90	6.17	49.0	2.02e+04	28.5	5
118	Pal13	87.10	-42.70	24.5	25.6	1.00	2.82	28.2	5.12e+03	13.0	4
119	NGC7492	53.39	-63.48	25.0	24.2	1.00	6.17	61.7	5.56e+04	-188.5	8

REFERENCES.— (1) Pryor & Meylan 1993 (in case of multiple choice, mean values are assumed); (2) Da Costa & Armandroff 1995; (3) Geisler et al. 1995; (4) Kulessa & McDowell 1985; (5) Armandroff & Da Costa 1991; (6) Cannon 1993; (7) Da Costa, Armandroff, & Norris 1992; (8) Webbink 1981; (9) Hesser, Shawl, & Meyer 1986; (10) Zaritsky et al. 1989; (11) Suntzeff, Olszewski, & Stetson 1985; (12) Peterson, Seitzer, & Cudworth 1989; (13) Peterson, & Cudworth 1994; (14) Peterson, Rees, & Cudworth 1995; (15) Zinn & West 1984; (16) Schweitzer, Cudworth, & Majewski 1993.

TABLE 3
DESTRUCTION RATES FOR CLUSTERS IN SAMPLE^a

ID	Name	t_{rh} (yr)	ν_{evap}	OC isotropic			BSS isotropic		
				ν_{d1+d2}	ν_{d1+b1}	ν_{tot}	ν_{d1+d2}	ν_{d1+b1}	ν_{tot}
1	NGC0104	3.94e+09	7.10e-02	7.84e-02	7.36e-02	7.91e-02	1.37e-01	1.11e-01	1.49e-01
2	NGC0288	1.42e+09	3.71e-01	4.03e-01	4.47e+00	1.93e+01	8.80e-01	6.37e-01	1.10e+00
3	NGC0362	1.18e+09	2.18e-01	2.28e-01	2.24e-01	2.33e-01	3.34e-01	2.85e-01	3.54e-01
4	NGC1261	1.51e+09	2.33e-01	2.39e-01	2.39e-01	2.48e-01	2.74e-01	2.50e-01	2.79e-01
5	Pal1	6.87e+07	4.37e+00	5.34e+00	1.39e+01	2.26e+01	4.47e+00	4.47e+00	4.49e+00
6	AM1	1.72e+09	2.20e-01	4.03e-01	3.80e-01	6.02e-01	2.20e-01	2.20e-01	2.20e-01
7	Eridanus	2.16e+09	2.03e-01	2.07e-01	2.04e-01	2.06e-01	2.03e-01	2.03e-01	2.03e-01
8	Pal2	2.87e+08	1.06e+00	1.06e+00	1.09e+00	1.08e+00	1.06e+00	1.06e+00	1.06e+00
9	NGC1851	2.72e+09	1.24e-01	1.27e-01	1.25e-01	1.27e-01	1.28e-01	1.26e-01	1.24e-01
10	NGC1904	8.77e+08	2.83e-01	2.85e-01	2.84e-01	2.84e-01	3.40e-01	3.10e-01	3.54e-01
11	NGC2298	3.36e+08	1.02e+00	1.02e+00	1.02e+00	1.05e+00	1.03e+00	1.02e+00	1.03e+00
12	NGC2419	3.90e+10	7.97e-03	8.00e-03	7.98e-03	7.99e-03	7.97e-03	8.03e-03	8.01e-03
13	NGC2808	2.30e+09	1.16e-01	1.10e-01	1.10e-01	1.11e-01	1.50e-01	1.32e-01	1.61e-01
14	Pal3	8.46e+09	5.88e-02	5.88e-02	5.88e-02	5.88e-02	5.88e-02	5.88e-02	5.88e-02
15	NGC3201	1.62e+09	2.07e-01	2.63e-01	2.28e-01	2.69e-01	3.30e-01	2.65e-01	3.45e-01
16	Pal4	7.38e+09	1.16e-01	1.16e-01	1.16e-01	1.16e-01	1.16e-01	1.16e-01	1.16e-01
17	NGC4147	5.00e+08	4.83e-01	4.84e-01	4.84e-01	4.84e-01	4.83e-01	4.83e-01	4.83e-01
18	NGC4372	2.76e+09	1.24e-01	1.48e-01	1.36e-01	1.58e-01	4.59e-01	3.04e-01	4.74e-01
19	Rup106	1.64e+09	5.03e+00	7.88e+00	6.00e+00	7.97e+00	5.11e+00	5.05e+00	5.13e+00
20	NGC4590	3.56e+09	7.17e-02	1.08e-01	8.16e-02	9.82e-02	8.12e-02	7.55e-02	8.22e-02
21	NGC4833	7.86e+08	4.52e-01	4.83e-01	5.91e-01	7.65e-01	1.60e+00	2.40e+00	4.36e+00
22	NGC5024	8.74e+09	2.88e-02	2.84e-02	2.88e-02	2.88e-02	3.03e-02	2.96e-02	3.07e-02
23	NGC5053	6.76e+09	1.07e-01	2.46e+00	4.81e+00	1.39e+01	1.36e+00	2.40e-01	1.62e+00
24	NGC5139	1.01e+10	3.65e-02	6.58e-02	1.01e-01	1.60e-01	1.49e-01	1.92e-01	3.43e-01
25	NGC5272	7.28e+09	3.41e-02	4.01e-02	3.66e-02	3.98e-02	5.19e-02	4.29e-02	5.42e-02
26	NGC5286	7.42e+08	3.97e-01	4.00e-01	3.96e-01	4.01e-01	4.57e-01	1.07e+00	1.57e+00
27	NGC5466	1.57e+10	1.88e-02	1.02e+00	4.69e-01	3.01e+00	1.66e+00	4.30e-01	2.73e+00
28	NGC5634	2.27e+09	1.18e-01	1.18e-01	1.17e-01	1.19e-01	1.15e-01	1.18e-01	1.15e-01
29	NGC5694	1.17e+09	2.13e-01	2.11e-01	2.17e-01	2.13e-01	2.10e-01	2.10e-01	2.10e-01
30	IC4499	4.26e+09	9.93e-02	1.07e-01	1.02e-01	1.11e-01	4.57e-01	2.34e-01	4.76e-01
31	NGC5824	2.13e+10	1.96e-02	2.08e-02	2.02e-02	2.10e-02	2.71e-02	2.41e-02	3.06e-02
32	Pal5	7.17e+09	1.64e-01	2.37e+00	3.79e+00	9.62e+00	1.74e-01	1.66e-01	2.16e-01
33	NGC5897	3.96e+09	2.05e-01	1.49e+00	6.55e+00	1.85e+01	3.71e+01	1.63e+02	4.18e+02
34	NGC5904	3.75e+09	6.76e-02	8.61e-02	8.57e-02	1.08e-01	4.06e-01	1.11e+00	1.76e+00
35	NGC5927	1.32e+09	1.98e-01	2.23e-01	2.14e-01	2.43e-01	3.57e-01	2.71e-01	3.49e-01
36	NGC5946	6.36e+09	6.80e-02	1.73e-01	2.17e-01	3.43e-01	2.32e-01	1.46e-01	2.38e-01
37	NGC5986	1.76e+09	2.13e-01	2.20e-01	9.37e-01	1.74e+00	5.42e-01	1.81e+00	9.70e+00
38	Pal14	7.90e+09	1.78e-01	1.78e-01	1.83e-01	1.96e-01	3.97e+00	9.41e+00	2.05e+01
39	NGC6093	9.26e+08	2.77e-01	2.84e-01	2.88e+00	4.20e+00	7.68e-01	1.35e+00	1.86e+00
40	NGC6101	1.96e+09	3.97e-01	4.05e-01	4.00e-01	4.05e-01	9.38e+00	1.32e+01	3.76e+01
41	NGC6121	3.70e+08	7.05e-01	7.16e-01	7.54e-01	8.30e-01	7.38e-01	7.37e-01	7.52e-01
42	NGC6144	2.10e+09	1.65e-01	3.26e-01	4.78e-01	7.21e-01	1.71e+00	9.30e-01	2.00e+00
43	NGC6139	5.40e+08	4.53e-01	4.56e-01	4.55e-01	4.61e-01	7.13e-01	2.16e+00	3.07e+00
44	NGC6171	8.48e+08	3.26e-01	3.57e-01	3.40e-01	3.77e-01	5.59e-01	4.22e-01	5.48e-01
45	NGC6205	3.17e+09	9.13e-02	1.23e-01	1.15e-01	1.47e-01	1.01e-01	9.55e-02	1.02e-01
46	NGC6218	1.01e+09	3.13e-01	3.16e-01	3.87e-01	4.68e-01	3.78e-01	3.39e-01	3.84e-01
47	NGC6229	2.06e+09	1.41e-01	1.28e-01	1.27e-01	1.28e-01	1.27e-01	1.28e-01	1.31e-01
48	NGC6235	5.30e+08	6.18e-01	6.20e-01	6.78e+00	3.26e+01	9.06e-01	7.99e-01	1.02e+00

TABLE 3—*Continued*

ID	Name	t_{rh} (yr)	ν_{evap}	OC isotropic			BSS isotropic		
				ν_{d1+d2}	ν_{d1+b1}	ν_{tot}	ν_{d1+d2}	ν_{d1+b1}	ν_{tot}
49	NGC6254	7.60e+08	4.01e-01	4.33e-01	4.51e-01	5.03e-01	4.22e-01	4.08e-01	4.23e-01
50	NGC6256	4.67e+08	8.68e-01	8.95e-01	9.72e-01	1.08e+00	1.76e+00	1.29e+00	1.78e+00
51	Pal15	3.33e+09	3.80e+02	3.80e+02	3.80e+02	3.80e+02	3.81e+02	3.81e+02	3.83e+02
52	NGC6266	4.09e+08	6.27e-01	6.28e-01	6.33e-01	6.44e-01	6.26e-01	6.31e-01	6.38e-01
53	NGC6273	3.29e+09	9.68e-02	9.24e-02	1.02e-01	1.20e-01	2.89e-01	4.72e+00	2.46e+01
54	NGC6284	4.82e+09	8.68e-02	4.69e-01	3.79e-01	5.98e-01	2.26e+00	3.11e+00	5.34e+00
55	NGC6287	3.01e+08	8.88e-01	8.70e-01	1.52e+00	2.09e+00	9.78e-01	9.62e-01	1.13e+00
56	NGC6293	1.45e+09	2.88e-01	3.02e-01	6.88e+00	9.66e+00	1.47e+00	6.21e+00	9.05e+00
57	NGC6304	4.08e+08	5.94e-01	6.08e-01	2.91e+00	4.37e+00	6.60e-01	6.22e-01	6.74e-01
58	NGC6316	8.97e+08	3.10e-01	3.06e-01	6.71e-01	9.61e-01	3.31e-01	3.09e-01	3.13e-01
59	NGC6325	3.08e+08	1.33e+00	1.35e+00	2.52e+00	3.54e+00	1.66e+00	1.45e+00	1.67e+00
60	NGC6341	9.27e+08	2.65e-01	2.68e-01	2.64e-01	2.66e-01	3.60e-01	3.25e-01	4.01e-01
61	NGC6333	6.57e+08	6.15e-01	6.18e-01	6.19e-01	6.26e-01	7.24e-01	1.82e+00	3.11e+00
62	NGC6342	2.36e+09	1.80e-01	3.23e-01	3.09e-01	4.53e-01	1.66e+00	3.55e+00	5.27e+00
63	NGC6356	1.94e+09	1.44e-01	1.43e-01	1.44e-01	1.43e-01	1.82e-01	1.59e-01	1.83e-01
64	NGC6355	1.52e+09	2.79e-01	2.96e-01	3.78e-01	4.89e-01	9.20e-01	1.59e+00	2.47e+00
65	NGC6352	5.33e+08	8.02e-01	8.14e-01	8.06e-01	8.14e-01	1.04e+00	8.93e-01	1.05e+00
66	NGC6366	4.20e+08	1.37e+00	1.41e+00	1.45e+00	1.63e+00	3.25e+00	3.13e+00	8.64e+00
67	NGC6362	1.48e+09	2.90e-01	4.26e-01	3.64e-01	4.78e-01	7.29e-01	4.60e-01	7.35e-01
68	NGC6388	8.25e+08	3.08e-01	3.07e-01	3.08e-01	3.16e-01	3.22e-01	3.18e-01	3.53e-01
69	NGC6402	8.68e+09	3.08e-02	7.99e-02	4.72e+00	2.06e+01	2.65e-01	2.17e-01	3.32e-01
70	NGC6401	8.78e+08	2.89e-01	2.90e-01	7.69e-01	1.09e+00	2.97e-01	3.02e-01	3.00e-01
71	NGC6397	1.76e+08	2.35e+00	2.36e+00	2.36e+00	2.42e+00	2.43e+00	2.37e+00	2.48e+00
72	NGC6426	1.61e+09	1.51e-01	2.54e-01	2.25e-01	3.14e-01	1.77e-01	1.63e-01	1.86e-01
73	NGC6440	2.87e+08	8.77e-01	8.78e-01	8.78e-01	8.89e-01	9.01e-01	8.98e-01	9.05e-01
74	NGC6441	1.04e+09	2.64e-01	2.42e-01	3.39e-01	4.28e-01	2.74e-01	2.57e-01	2.86e-01
75	NGC6453	2.81e+09	1.51e-01	8.28e-01	8.88e-01	1.38e+00	3.51e+00	2.40e+00	3.66e+00
76	NGC6496	2.14e+08	3.85e+01	3.86e+01	1.69e+02	3.36e+02	5.97e+01	1.55e+02	3.05e+02
77	NGC6517	7.21e+07	3.37e+00	3.37e+00	3.50e+00	3.46e+00	3.46e+00	3.37e+00	3.40e+00
78	NGC6522	8.28e+08	4.98e-01	8.31e-01	3.24e+00	5.04e+00	5.23e+00	6.08e+00	9.18e+00
79	NGC6535	2.45e+08	1.37e+00	1.40e+00	1.54e+00	1.79e+00	1.81e+00	1.66e+00	1.97e+00
80	NGC6528	7.65e+08	4.57e-01	6.90e-01	1.99e+00	3.00e+00	2.65e+00	2.58e+00	3.89e+00
81	NGC6539	4.81e+08	5.47e-01	5.44e-01	5.37e-01	5.49e-01	5.83e-01	5.54e-01	5.92e-01
82	NGC6544	1.62e+08	2.55e+00	2.55e+00	2.55e+00	2.55e+00	2.55e+00	2.55e+00	2.55e+00
83	NGC6541	2.57e+09	1.05e-01	1.80e-01	1.74e-01	2.42e-01	5.31e-01	4.50e-01	6.42e-01
84	NGC6553	1.94e+08	2.04e+00	2.04e+00	2.04e+00	2.10e+00	2.05e+00	2.04e+00	2.05e+00
85	NGC6558	1.09e+09	3.85e-01	3.93e-01	1.52e+00	2.41e+00	2.56e+00	3.74e+01	5.57e+01
86	NGC6569	6.09e+08	5.82e-01	5.80e-01	1.35e+00	2.01e+00	9.62e-01	5.96e+00	3.05e+01
87	NGC6584	9.72e+08	4.02e-01	4.03e-01	4.41e-01	5.18e-01	6.82e-01	6.28e-01	8.54e-01
88	NGC6624	2.68e+09	1.58e-01	1.62e-01	1.32e+00	1.83e+00	1.86e+00	2.79e+00	3.94e+00
89	NGC6626	4.84e+08	5.22e-01	5.28e-01	5.29e-01	5.46e-01	6.96e-01	1.09e+00	1.49e+00
90	NGC6638	2.70e+08	1.12e+00	1.13e+00	8.22e+00	1.41e+01	1.70e+00	3.07e+00	4.39e+00
91	NGC6637	8.03e+08	3.88e-01	3.91e-01	1.21e+00	1.81e+00	5.37e-01	4.63e-01	5.45e-01
92	NGC6642	3.81e+08	6.69e-01	7.03e-01	1.38e+00	1.90e+00	1.88e+00	4.03e+00	5.56e+00
93	NGC6652	3.51e+08	7.08e-01	6.95e-01	7.08e-01	7.28e-01	6.96e-01	6.94e-01	6.95e-01
94	NGC6656	1.12e+09	3.03e-01	3.11e-01	3.06e-01	3.15e-01	3.24e-01	3.09e-01	3.21e-01
95	Pal8	1.18e+09	8.70e-01	8.72e-01	8.71e-01	8.72e-01	8.70e-01	8.70e-01	8.70e-01
96	NGC6681	6.75e+08	6.34e-01	6.26e-01	6.51e-01	7.09e-01	8.55e-01	1.06e+00	1.48e+00

TABLE 3—*Continued*

ID	Name	t_{rh} (yr)	ν_{evap}	OC isotropic			BSS isotropic		
				ν_{d1+d2}	ν_{d1+b1}	ν_{tot}	ν_{d1+d2}	ν_{d1+b1}	ν_{tot}
97	NGC6712	6.94e+08	8.54e-01	8.57e-01	1.03e+00	1.35e+00	1.16e+00	7.46e+00	3.59e+01
98	NGC6715	2.72e+09	9.24e-02	9.41e-02	9.41e-02	9.56e-02	1.83e-01	2.90e-01	4.03e-01
99	NGC6717	3.44e+08	8.15e-01	7.99e-01	6.04e+00	8.97e+00	1.80e+00	4.30e+00	6.13e+00
100	NGC6723	1.60e+09	2.93e-01	2.97e-01	2.96e-01	3.21e-01	5.04e-01	4.09e-01	5.77e-01
101	NGC6752	4.61e+09	9.19e-02	2.40e-01	1.60e-01	2.44e-01	3.08e-01	2.04e-01	3.23e-01
102	NGC6760	3.99e+08	6.45e-01	6.87e-01	6.69e-01	7.16e-01	9.49e-01	8.86e-01	1.11e+00
103	Terzan7	3.55e+09	1.24e-01	1.26e-01	1.29e-01	1.28e-01	1.28e-01	1.25e-01	1.25e-01
104	NGC6779	6.46e+08	4.86e-01	4.90e-01	4.88e-01	5.01e-01	5.21e-01	5.12e-01	5.24e-01
105	Arp2	5.75e+09	1.04e-01	1.21e-01	1.22e-01	1.61e-01	3.59e+01	1.94e+01	6.02e+01
106	NGC6809	1.64e+09	5.84e-01	6.03e-01	6.42e-01	7.52e-01	6.67e-01	6.06e-01	6.83e-01
107	Terzan8	9.94e+08	1.27e+03	1.28e+03	1.28e+03	1.28e+03	1.28e+03	1.28e+03	1.28e+03
108	Pal11	3.07e+09	7.62e+00	1.21e+01	9.16e+00	1.21e+01	1.36e+01	9.85e+00	1.38e+01
109	NGC6838	1.22e+08	3.40e+00	3.33e+00	3.41e+00	3.34e+00	3.34e+00	3.35e+00	3.34e+00
110	NGC6864	1.35e+09	1.87e-01	1.91e-01	1.88e-01	1.92e-01	1.91e-01	1.88e-01	1.89e-01
111	NGC6934	1.01e+09	2.80e-01	2.74e-01	2.74e-01	2.75e-01	2.85e-01	2.77e-01	2.89e-01
112	NGC6981	2.11e+09	1.73e-01	1.79e-01	1.74e-01	1.76e-01	1.83e-01	1.74e-01	1.76e-01
113	NGC7006	3.43e+09	8.72e-02	8.96e-02	8.83e-02	9.02e-02	8.72e-02	8.73e-02	8.72e-02
114	NGC7078	7.01e+09	6.23e-02	1.18e-01	1.35e-01	2.03e-01	2.02e-01	1.38e-01	2.17e-01
115	NGC7089	4.52e+09	5.51e-02	7.59e-02	6.74e-02	8.13e-02	5.85e-02	5.66e-02	5.76e-02
116	NGC7099	1.77e+09	2.38e-01	2.70e-01	2.55e-01	2.88e-01	4.65e-01	4.04e-01	5.65e-01
117	Pal12	1.52e+09	3.98e-01	4.12e-01	4.12e-01	4.15e-01	3.79e+00	1.06e+00	7.12e+00
118	Pal13	3.34e+08	1.57e+00	1.57e+00	1.57e+00	1.57e+00	1.57e+00	1.57e+00	1.57e+00
119	NGC7492	2.75e+09	1.85e-01	2.24e-01	2.28e-01	3.16e-01	4.72e+00	3.79e+00	1.44e+01

^aDestruction rates ν in units of inverse Hubble time.

NOTE.—The rates including the tidal shocks are: ν_{d1+d2} – first and second order disk shock, ν_{d1+b1} – first order disk and bulge shocks, ν_{tot} – total destruction rate (first and second order disk+bulge shocks). The two groups of columns correspond to the results for the OC and BSS galactic models. In both cases the isotropic kinematic model is assumed, appropriate for the present clusters. The Weinberg’s form of the adiabatic correction is used (see text for more detail).